Proterozoic evolution of the phosphorus cycle: Was it high or was it low?

Romain Guilbaud

Proterozoic evolution of the phosphorus cycle: was it high or was it low?

Romain Guilbaud

Centre National de la Recherche Scientifique (CNRS)

Laboratoire Géosciences Environnement Toulouse (UMR 5563)

Observatoire Midi-Pyrénées, Toulouse, France

Abstract

The Proterozoic eon witnessed the emergence of eukaryotes and the protracted oxygenation of the Earth's surface. In that regard, phosphorus, considered the limiting nutrient on geologic timescales, may have played a substantial role, as it links to the biogeochemical cycle of carbon and to the evolution of life. However, reconstructing its bioavailability through the Proterozoic is difficult, as it relies on limited evidence from the rock record, with no direct estimation of seawater phosphorus levels. Here, I will review and discuss current debates and try to identify the main limitations of our understanding of the Proterozoic phosphorus paradigms.

Keywords

Phosphorus; Proterozoic; Biogeochemistry; Nutriment; Oxygen; Carbon; Iron; Redox; Cycles; Reconstruction; Redfield; Eukaryotes; Oxygenation.

Key points/Objectives

- Summary of knowledge and paradigms from modern analogues
- Overview of the classical approaches to determine P cycling in the deep past, and their limitations
- Overview of recent approaches and new paradigms emerging from these approaches
- Concluding remarks

1. Introduction

Phosphorus (P) and nitrogen (N) are the two major nutrients essential to all forms of life. P plays a central role in biochemistry as it occurs within metabolic molecules (ATP), the structure of cell membranes (as phospholipids) and nucleic acids (DNA, RNA). Therefore, it is widely assumed that its key function emerged early in the building blocks of life. Whilst N availability to marine organisms may be sporadically limited by the extent of biological fixation of gaseous N, its atmospheric reservoir is practically infinite. By contrast, the reservoir of dissolved marine P is controlled by three factors: the source of P to the ocean, i.e. the flux of continental crust weathering; the removal flux of P to the sediment, diminishing its availability in the ocean; and the potential redox-promoted recycling of P back to the water column, nuancing the efficiency of P removal to the sediment. Moreover, marine P bioavailability is quite different to dissolved phosphate concentrations in seawater, as there is a range of reactive P-bearing particles and colloids that may also be utilised by organisms. Therefore, understanding the speciation of both solid and dissolved P in the water column and the sediments becomes substantial to evaluate the extent of P bioavailability.

All in all, P is generally considered the ultimate limiting nutrient on geological timescales (Tyrrell, 1999), with direct implications on primary production. In turn, the extent of biomass derived from primary production exerts control on the flux of organic carbon (C_{org}) to the sediment and, consequently, on C_{org} burial within the sediment. C_{org} burial is commonly considered a source of atmospheric oxygen, since the utilisation of the latter during oxidative decay of organic matter becomes muted when C_{org} gets buried on the long term. Hence, on geologic timescales, it is generally assumed that the cycle of P directly links with primary producers and, ultimately, atmospheric oxygen, although this P-O_2 coupling has been recently questioned for the Precambrian (Dodd et al., 2023).

Considering this shared history amongst surface weathering processes, phosphorus bioavailability, life itself, and oxygen production, the Proterozoic eon (2.5 to 0.541 billion years ago, Ga) plays a central role. Indeed, it witnessed several of the most important revolutions in Earth history, such as the protracted oxygenation of the oceans and the atmosphere in the early Proterozoic (Farquhar et al., 2000; Bekker et al., 2004), the rise and evolution of early eukaryotes (Martin et al., 2003; Knoll et al., 2006; Javaux, 2011), and the emergence of animal life in the terminal Proterozoic, which changed forever the world's biosphere dynamics (Knoll and Carroll,

1999; Butterfield, 2009). In that sense, the Proterozoic may be considered the cradle of our modern habitat, and consequently, 'chicken and eggs' questions around the evolutionary steps that lead to the Phanerozoic remain largely debated.

This is certainly the case regarding the phosphorus reservoirs, cycling, and bioavailability, with studies suggesting high marine phosphorus throughout most of the Proterozoic (e.g., Planavsky et al., 2010) whilst others argue in favour of the opposite (e.g., Reinhard et al., 2017). In what follows, I attempt to summarise our current understanding and limitations on how and why the global P reservoir evolved in the Proterozoic while highlighting how experiments may help us tackle this question.

1.1. Phosphorite deposits and the oxygenation of the Earth's surface

Our current understanding of the oxygenation of the Earth's surface suggests that the atmosphere and the major part of the oceans remained anoxic until the Great Oxidation Event (GOE), which occurred ~2.4-2.2 Ga (Bekker et al., 2004; Lyons et al., 2014; Poulton et al., 2021), with 'whiffs' of oxygen predating the GOE (Anbar et al., 2007; Kaufman et al., 2007; Scott et al., 2008; Kendall et al., 2010). This unprecedented episode, during which our atmosphere switched from being reducing to oxidising, marked what may well have been the most decisive event for our planet's biosphere. As oxidative weathering can dig out a range of reduced species from the continental crust, one of the first and notable consequences of the GOE is a dramatic change in weathering regime and nutrient influxes to the oceans.

Phosphorus contents in the upper continental crust, given as P_2O_5, cluster around 0.15 wt% (Rudnick and Gao, 2003). Weathering of the continental crust being the ultimate source of phosphorus to the oceans, one may expect to recover eventually similar contents in marine sediments, over geologic timescales. Whereas the average deep sea clays yield similar P contents (Turekian and Wedepohl, 1961), other marine sedimentary rocks significantly deviate from that value, suggesting that a range of biogeochemical processes may store P in the sediments or, by contrast, regenerate and accumulate P in the water column. Phosphorites, for instance, are sedimentary deposits that consist of >10 wt% P (Holland, 2005), either disseminated within shales, or occurring as discrete nodules, lenses or layers of apatite. Figure 1 shows the evolution of phosphorite deposits and the oxygenation of the Earth's surface. Notably, early Earth's marine sedimentary rocks are characterized by a lack of both phosphorite deposition and atmospheric oxygen. It is during the Palaeoproterozoic (2.5 to 1.6 Ga), and more precisely during the Lomagundi event (~2.22 to 2.06 Ga), which records a large positive C isotope excursion and presumably marks the stabilisation of the non-reversable oxidised atmosphere (Poulton et al., 2021), that the first economic phosphorites deposited (Bekker and Holland, 2012). Phosphorite deposits are then found discontinuously and in lesser abundances until a second, Neoproterozoic

rise in atmospheric oxygen, where phosphorite abundances increase again (Fig. 1). The synchronicity between the history of atmospheric oxygen and the geologic record of phosphate-rich sedimentary rocks (Papineau, 2010) not only reminds us that, as a major nutrient, P somehow links to C_{org} production and burial and, eventually, to the degassing of atmospheric oxygen (Alcott et al., 2019), but also that in order to reconstruct its past cycling and bioavailability, one has to scrutinise the redox evolution of the oceans, in other words, the scene where P dynamics took place.

1.2. A brief history of the redox evolution of the Precambrian oceans

The common hypothesis for the rather late Earth's surface oxygenation – over 1 Ga after the putative emergence of oxygenic photosynthesising cyanobacteria (Schopf, 1993; Rosing et al., 1996; Brasier et al., 2002) – is that early oxygen oases derived from photosynthesis first reacted with vast amounts of dissolved ferrous iron (Fe) in anoxic and Fe-rich (ferruginous) oceans, prior to accumulating and degassing into the atmosphere (Olson et al., 2013). This led to the intermittent deposition of laminated, iron-rich, chemical sediments (so called 'banded iron formations, 'BIFs'), from the Archean to ~1.9 Ga (Fig. 1).

The progressive oxygenation of the atmosphere, from the Archean 'whiffs' to the GOE, enhanced the input fluxes of sulphate to the ocean due to oxidative weathering of continental sulphides (Canfield, 1998). Higher sulphate influxes on productive, continental margins favoured higher rates of bacterial sulphate reduction, leading to a significant increase in the extent of euxinic (anoxic and sulphide-rich, Fig. 2) waters by ~1.8 Ga (Canfield, 1998; Poulton et al., 2004a, 2010), coinciding with the cessation of BIF deposition (Figs. 1 & 2). Note that the last episode of BIF deposition occurred in between the first and second episodes of phosphorite deposition, suggesting that conditions favouring BIF deposition may have hampered the accumulation of P in the ocean, which I will discuss later.

Atmospheric oxygen models indicate that after the GOE, pO_2 remained well below the present atmospheric level (PAL), with estimates ranging from <0.001 to ~0.4 PAL (Kump, 2008; Planavsky et al., 2014; Zhang et al., 2016). Whilst the deeper ocean remained mostly ferruginous (Poulton and Canfield, 2011; Planavsky et al., 2011), it is thought that euxinic conditions were prevalent in mid-depths environments of continental margins and intracratonic basins, and so until the early Neoproterozoic (~1 to 0.8 Ga). During this 'boring billion' of evolutionary stasis (Knoll et al., 2006; Javaux, 2011), it is widely assumed that atmospheric oxygen also remained at relatively constant levels (Fig. 1; Kump, 2008; Lyons et al., 2014; Planavsky et al., 2014). However, evidence for fluctuations in both the extent of ocean oxygenation (Doyle et al., 2018; Zhang et al., 2018) and the global-scale nature of ocean redox conditions (Guilbaud et al., 2015; Sperling et al., 2015)

could suggest variations in atmospheric oxygen concentrations, divorcing from the idea of constant O_2 levels through that interim.

In the early Neoproterozoic (1 to 0.8 Ga), euxinic conditions became anecdotical (Guilbaud et al., 2015; Sperling et al., 2015; but see also Dahl et al., 2011; Thomson et al., 2015). Isotope evidence for expansive oxic conditions in surface waters after 0.8 Ga (Planavsky et al., 2014) may also depict the deepening of the redoxcline at that time. In the later Neoproterozoic (~0.8 to 0.541 Ga), the redox structure of the oceans seem to have oscillated from ferruginous to oxic conditions, with sulphidic conditions due to higher sulphate levels being restricted to the sediment (Canfield et al., 2007, 2008; Johnston et al., 2010; Wood et al., 2015; Tostevin et al., 2019) during the protracted establishment of modern-like oxygen minimum zones at the Proterozoic-Cambrian transition (Tostevin et al., 2016; Guilbaud et al., 2018, Fig. 2).

1.3. Questioning the paradigms

The observation that the atmosphere never returned to anoxic conditions after ~2.22 Ga (Poulton et al., 2021), but that oxygen levels remained persistently low throughout most of the Earth's 'middle age' (Kump, 2008; Lyons et al., 2014; Guilbaud et al., 2020), suggests that C_{org} burial was somehow muted throughout that interval. Several fundamental questions remain open on why and how. For instance, muted C_{org} burial may suggest nutrient limitations on primary production; hence, the question is what role did phosphorous play in that story? Was phosphorus a limiting factor for the early evolution of eukaryotic life? Did organisms uptake P in their organic tissues in the same proportions as today? Were the intrinsic dynamics of the cycles of phosphorus, carbon and oxygen as described through the Phanerozoic (Berner, 1989; Berner and Canfield, 1989) equally operating during the Proterozoic?

In order to address these questions, section 2 will summarize our understanding of the P cycle in modern settings, sometimes considered as analogues to Proterozoic environments. Sections 3, 4 and 5 will explore and question our ability to reconstruct seawater P levels and P dynamics from the rock record.

2. Insights form the modern P cycle in marine environments

There has been extensive work since the '80s on the phosphorus cycle in modern environments. My aim here is not to review that work, as such exhaustive reviews already exist (i.e., Ruttenberg, 2003), but to extract the main aspects of P dynamics in a range of environments that may help us reconstruct the P cycle in ancient environments.

2.1. Oxic water columns

In the modern, dominantly oxidised environment (with >250 μM dissolved O_2 in seawater), marine dissolved P commonly occurs as orthophosphate. It is sourced from the weathering of the continental crust through riverine fluxes, as neither hydrothermal vents nor the alteration of the oceanic crust deliver significant amounts of P to the ocean (Wheat et al., 1996). Phosphorus is particle reactive, and its transport by rivers is mainly associated with a range of particles, broadly distributed into organic matter, ferric (oxyhydr)oxides and apatite, while the residual dissolved riverine pool is by half comprised of dissolved organics (Ruttenberg and Canfield, 1994; Ruttenberg, 2003).

Once in the marine environment, phosphorus is removed from the ocean through particle transport to the seafloor and sediment burial (Frohlich et al., 1982; Ruttenberg, 1992, 2003; Delaney, 1998). Dissolved orthophosphate may be directly taken up by phytoplankton, hence incorporating organic matter, with a remarkably constant atomic C:P ratio of 106:1, canonically referred to as the 'Redfield ratio' due to its discoverer (Redfield, 1958). In fact, for fresh phytoplankton, this ratio actually shows some degree of variability, due to local nutrient availability (Goldman et al., 1979; Anderson and Sarmiento, 1994; Lenton and Watson, 2000; Teng et al., 2014); yet, organisms may use enzymatic pathways to reach out phosphorus from reactive particles when dissolved phosphate becomes depleted (Ruttenberg, 2003). Then, the produced dissolved organic phosphorus pool also plays a considerable but highly variable part of the total dissolved P that is available to organisms (Björkman and Karl, 2003; Lomas et al., 2010; Karl and Björkman, 2015). During deposition, up to 90% of C_{org} may be remineralised through organic matter respiration, releasing organic-bound P back to the water column. By contrast, as sinking Fe (oxyhydr)oxdides are efficient P scavengers, their deposition act as a P removal carrier to the sediment. Similarly, without the presence of free dissolved Fe(II), detrital apatite remains fairly insoluble in oxic waters (Brady et al., 2022) and also consists in a major P carrier to the sediment. In addition to these three P transport pathways to the seabed (i.e., organic matter, Fe (oxyhydr)oxides and detrital apatite), authigenic minerals of abiotic or biogenic origin, such as carbonates and carbonate fluorapatite (CFA), may form in the water column and sink down along with detrital particles and, to a lesser extent, dust (Frohlich et al., 1982; Ruttenberg, 1992; Ruttenberg and Berner, 1993; Ruttenberg and Canfield, 1994; Delaney, 1998).

2.2. Oxygen-depleted sediments underneath oxic waters

Depending upon organic matter loading at the sediment-water interface, respiration processes result in the rapid exhaustion of dissolved O_2 in the sediment, or sometimes directly above it (Canfield and Thamdrup, 2009). Organic matter mineralisation then involves other electron acceptors than oxygen such as, amongst others, nitrate, Fe (oxyhydr)oxides and sulphate. During bacterial Fe reduction in the sediment, produced Fe^{2+} subsequently reprecipitates as

authigenic ferric oxyhydroxides at the sediment-water interface, which may re-adsorb phosphorus released during organic matter respiration (Slomp et al., 1996a). In turn, depending on the rates of Fe reduction, P may be released and trapped as authigenic CFA in porewaters, and therefore Fe minerals play a key role in CFA precipitation during early diagenesis (Jarvis et al., 1994; Slomp et al., 1996a, Fig. 3).

When sulphide is produced in the sediment during sulphate reduction, Fe (oxyhydr)oxides get rapidly dissolved by HS^- or H_2S (Pyzik and Sommer, 1981; Canfield et al., 1992; Dos Santos Afonso and Stumm, 1992; Peiffer et al., 1992; Poulton, 2003; Poulton et al., 2004b), producing Fe sulphides, which are significantly less efficient at adsorbing or coprecipitating P (Krom and Berner, 1980, 1981). This results in the release of Fe-bound phosphorus, itself augmented by the preferential release of P during organic matter degradation by sulphide (Ingall et al., 1993; Van Cappellen and Ingall, 1994; Ingall and Jahnke, 1997; Slomp et al., 2004; Mort et al., 2010). Depending on the extent of sulphidation, released phosphorus is partly regenerated to porewaters and the water masses above, although this regeneration is nuanced by the formation of vivianite ($Fe^{II}_3(PO_4)_2{\cdot}8H_2O$) at the interface where sulphide has been consumed and where Fe(II) is produced, reacting with dissolved phosphate (Slomp et al., 2013, p.2013; Hsu et al., 2014; Egger et al., 2015; Dijkstra et al., 2016; Liu et al., 2018; März et al., 2018; Xiong et al., 2019; Kubeneck et al., 2021), or during its incorporation into CFA (Jarvis et al., 1994; Filippelli and Delaney, 1996; Slomp et al., 1996a).

Degradation of C_{org} by the different redox regimes outlined above results in sedimentary C/P ratios departing from the Redfield ratio of 106:1 (Anderson et al., 2001), which also links to sedimentations rates (Ingall and Van Cappellen, 1990) and, subsequently, to the deposition depth (it be pelagic or on the shelf). For instance, oxic degradation at low sedimentation rates may favour the preferential decomposition of C_{org} over organic P, and a ratio close to or <106:1 (Ingall and Van Cappellen, 1990). By contrast, the preferential release of P_{org} when C_{org} degradation operates *via* sulphide reduction results in C_{org}/P_{org} ratios surpassing the Redfield ratio by orders of magnitude (Ingall and Jahnke, 1997), while they can remain close to the Redfield ratio in iron-dominated sediments (Ruttenberg and Goni, 1997). Slomp and Van Cappellen (2007, Fig. 4) summarized C_{org}/P_{org} data from a range of sediments, including some deposited under anoxic water columns, which I will cover below.

The assessment of the total P (P_{tot}) budget in sediments (e.g., Frohlich et al., 1982) have been significantly readdressed by the development of an operationally defined, sedimentary P extraction scheme ('SEDEX', Ruttenberg, 1992). The SEDEX method targets five sedimentary P pools including the loosely sorbed fraction (P_{sorb}), Fe (oxyhydr)oxides-bound P (P_{Fe1}), P associated

with authigenic apatite, biogenic apatite and carbonates (P_{auth}), detrital apatite and other unreactive inorganic P (P_{det}) and organic P (P_{org}). Hence, the SEDEX method allows an evaluation of the proportion of phosphorus that is well crystalline and remains unreactive to organisms during transport, deposition and burial (i.e., P_{det}), and the proportion of phosphorus that is reactive towards biogeochemical reactions and that is or may have been utilised by organisms. Such reactive phosphorus (here referred to as P_{reac}), is the sum of the other P pools extracted by the SEDEX method, such as $P_{reac} = P_{sorb} + P_{Fe1} + P_{auth} + P_{org}$. Further, the SEDEX method permits to evaluate the extent of 'P sink switches', which occur *via* the biogeochemical reactions listed above during early diagenesis. Therefore, it also allows the inspection of C_{org}/P_{reac} ratios, instead of C_{org}/P_{org}, which may account for the diagenetic transfers of phosphorus from organic matter to other reactive endmembers (Anderson et al., 2001). Note, however, that it presumes a quantitative transfer within each P_{reac} pool with no loss to the water column, and that it neglects the additional background influx of authigenic and Fe-bound phosphorus.

This summarised knowledge of the modern P cycle would suggest that we are well equipped to reconstruct the evolution of P reservoirs and P availability to organisms throughout Earth's history. Yet, ancient oceans were dominated by anoxic conditions, and the sedimentary rocks which may entail information on the P cycle in the deep past are limited. A range of modern, atypical environments, often (misleadingly) referred to as 'analogues' to ancient settings, may provide extremely insightful clues to the past. In these anoxic environments, the biogeochemical reactions that are usually restricted to anoxic sediments underneath oxic waters may start in the water column, at the redoxcline, and the nature of these reactions depends itself on the redox nature of the environment. So, how can our current understanding of the modern P cycle inform us about its past cycle, and where to find such atypical environments?

2.3. Ferruginous water columns

Ferruginous water columns refer to anoxic environments, either marine or lacustrine, which contain dissolved ferrous iron. In the modern world, these conditions are usually limited to stratified lakes where anoxia develops at depth. Under ferruginous conditions, highly reactive Fe particles commonly form within the water column, either by oxidation of ferrous Fe at the chemocline in the shallow waters, or by anoxygenic, photoautotrophic Fe(II) oxidising bacteria known as photoferrotrophs, also in the shallow photic zone (Kappler et al., 2005). In this context, bacterial P accumulation (Rivas-Lamelo et al., 2017) and P uptake by iron minerals such as ferrihydrite (Konhauser et al., 2007a) and green rust (a brucite-like mixed Fe(II)/Fe(III) hydroxide, with either carbonate or sulphate anions in the interlayer, *e.g.*, $Fe^{III}_2Fe^{II}_3(OH)_{12}CO_3$) starts in the water column, way above the sediment-water interface. This results in significant P

drawdown from the water column, and its accumulation in the sediment sink beneath (Zegeye et al., 2012; Cosmidis et al., 2014). Upon settling, P may be released to pore waters and the water column during anaerobic diagenesis, *via* partial decomposition of organic matter and the reduction of Fe (oxyhydr)oxides (Froelich et al., 1979; Krom et al., 1991; Ingall and Jahnke, 1997; Slomp et al., 2004). However, this process may be compensated by re-adsorption onto sinking Fe minerals at the sediment-water interface (Dellwig et al., 2010). This 'Fe wheel' (Busigny et al., 2016) likely enhances sedimentary P fixation in association with Fe minerals (Thompson et al., 2019), carbonates (Thompson, 2018; Rotaru et al., 2019; Vuillemin et al., 2019) or Fe phosphates (Slomp et al., 2013; Cosmidis et al., 2014; Egger et al., 2015; Xiong et al., 2019). This long term, P-fixation in sediments directly underneath ferruginous waters suggests that the subsequent sedimentary C_{org}/P_{reac} ratios may be closed to or below the Redfield ratio. However, studies of oligotrophic, ferruginous lake sediments show C/P ratios way above it (Thompson, 2018; Vuillemin et al., 2020), perhaps due to P limitations in the first place. The question remains whether ferruginous conditions with higher dissolved P concentrations yield similar results, or if P fixation into CFA or phosphates effectively occurs.

The wide range of P-associated Fe minerals, which surface chemistry and P sequestering abilities strongly differ from one mineral to another, suggests that the mineralogy of Fe-bearing particles exerts major controls on the fate of P under ferruginous conditions. In the oligotrophic ferruginous waters of Lake Towuti (Vuillemin et al., 2019) and Lake Matano (Crowe et al., 2008; Zegeye et al., 2012), where P:Fe(II) ratios range from 1:150 to 1:30, green rust is the dominant Fe mineral phase that forms in the water column, with subsequent transformation to more stable minerals, such as magnetite (Bauer et al., 2020) or siderite (Vuillemin et al., 2019). Vivianite formation is restricted to the deeper sediment, where Fe reduction allows the accumulation of P in the porewaters (Vuillemin et al., 2019). By contrast, in the phosphate-rich ferruginous waters of Lake Pavin, where phosphate concentrations reach up to 300 μM at the redoxcline (Cosmidis et al., 2014) with P:Fe(II) ratios ~1:6, and in the ferruginous porewaters of Lake Cadagno, with P:Fe(II) ratios ~1:3 (Xiong et al., 2019), the formation of vivianite commonly occurs (O'Connell et al., 2015), as early as in the water column (Cosmidis et al., 2014; Busigny et al., 2016).

Xiong et al. (2023) explored the mineralogical transformations occurring to Fe minerals when varying the P:Fe(II):Fe(III) proportions under anoxic conditions. They showed that for P:Fe(II) ratios <1:30, green rust is the sole crystalline phase observable in their experiments (Fig. 5a,b,c), and that P drawdown from the solution is operated by effective adsorption onto green rust particles and interlayer anion exchange, *via* the formation of amorphous Fe-P precursors which may delay the precipitation of crystalline green rust (Fig. 5c). For higher dissolved P and P:Fe(II) (Fig. 5d,e), green rust also forms but rapidly dissolves, however, leading to the formation of amorphous ferric (hydr)oxides together with dissolved Fe(II) and phosphate, with the dissolved

species subsequently reacting to form crystalline vivianite. These observations are in good agreement with studies showing the water column formation of green rust in modern oligotrophic, anoxic and Fe-rich settings, with vivianite forming when P accumulates to higher concentrations (Cosmidis et al., 2014; Bauer et al., 2020; Vuillemin et al., 2020).

2.4. Euxinic water columns

Contrasting with ferruginous settings, euxinic conditions refer to anoxic conditions containing dissolved sulphide, being dominantly represented by either H_2S or HS^-, depending upon local pH. The best example to illustrate such conditions in the modern world is certainly the Black Sea, where O_2 gets depleted at around 60m depth whilst sulphide starts building up at around 90m depth (Murray et al., 1989; Canfield and Thamdrup, 2009). Within that ~30m gap, nitrate, but mostly manganese (Mn) reduction operates (Canfield and Thamdrup, 2009), and particulate P is dominantly Mn oxide associated (Dijkstra et al., 2018b). In the deeper, euxinic waters, phosphorus recycling back to the water column gets particularly intense as most inorganic, oxide-bound P particles are dissolved by hydrogen sulphide and organic matter remains the main carrier of P to the sediment (Dijkstra et al., 2018b). Elevated sediment C_{org}/P_{org} ratios, surpassing the Redfield ratio (Dijkstra et al., 2014) further support preferential P release during C_{org} degradation by sulphate reduction (Ingall et al., 1993; Van Cappellen and Ingall, 1994; Ingall and Jahnke, 1997; Slomp et al., 2004). The SEDEX method revealed that whilst C_{org} gets consumed by microbial processes, P gets buried in the sediment as authigenic apatite and, surprisingly, in association with $CaCO_3$ (Dijkstra et al., 2014; Kraal et al., 2017). This, presumably, illustrates the absence of Fe minerals due to sulphide dissolution, and the lack of sedimentary Fe^{2+} production to react with phosphate to form vivianite.

Contrasting with the Black Sea, in low-sulphate, euxinic environments such as Lake Cadagno, hydrogen sulphide gets depleted, consumed by Fe within the first 20 cm of sediment (Xiong et al., 2019, Fig. 6). In such conditions, the combined fluxes of P and Fe^{2+} favour the supersaturation conditions required for vivianite formation in non-sulphidic part of the sediment (Xiong et al., 2019), similar to what is observed under the sulphate-methane transition sediments underneath oxic waters, or transiently euxinic bottom waters (Egger et al., 2015; Dijkstra et al., 2016; Liu et al., 2018; März et al., 2018). The persistence of vivianite in sulphide-rich environments was recently addressed by Dijkstra et al. (2018a), who confirmed experimentally that vivianite rapidly dissolves in sulphide-rich seawater (Vuillemin et al., 2013). Hence, its presence and effectiveness as a P sink in anoxic sediments highly depends upon sulphide contents and the dynamics of the sulphidation front within the sediment. In any case, the extent of P regeneration to the water column under euxinic conditions is likely linked to sulphate contents in the sediment, as they play a key role in promoting P retention as authigenic phases such as carbonates and phosphates. In

Lake Cadagno, C_{org}/P_{reac} considerably lower than C_{org}/P_{org} suggests that part of the recycled organic P gets sequestered by such phases (Xiong et al., 2019).

2.5. Conclusions arising from observations of the modern world

In the prospect of understanding P dynamics in the Proterozoic ocean, several aspects from modern, anoxic environments can be highlighted for further test against the rock record. In particular, I summarise the prime Fe and P mineralogy found in ferruginous and euxinic conditions in Table 1.

In the first instance, P drawdown may be efficient under ferruginous conditions, which have characterised most of the Proterozoic ocean (Poulton and Canfield, 2011; Planavsky et al., 2011), through Fe particle uptake to the sediment. While Fe reduction operates as early as in the water column, reactive Fe particles such as green rust are likely to adsorb or coprecipitate recycled P (Bauer et al., 2020; Xiong et al., 2023) under lower P concentrations. Under higher P concentrations, authigenic minerals such as vivianite may form (Cosmidis et al., 2014; Busigny et al., 2016; Xiong et al., 2023). Depending on P concentrations, despite P retention in the sediment *via* authigenic mineral fixation, C_{org}/P_{reac} ratios can be highly variable, from values close to the Redfield ratio (Ruttenberg and Goni, 1997) to values surpassing it (Vuillemin et al., 2019).

Under euxinic conditions, which developed along productive continental margins, as oxidative weathering enhanced the flux of sulphate to the oceans (Poulton et al., 2010; Poulton and Canfield, 2011), P recycling to the water column is favoured through both Fe reduction and C_{org} degradation (e.g., Slomp et al., 2004). This results in C_{org}/P_{org} ratios systematically >106:1; This recycling is, however, nuanced by the sediment fixation of P as authigenic apatite or in association with $CaCO_3$ in carbonate and sulphate rich environments (Kraal et al., 2017). In low-sulphate environments, which have characterized the Proterozoic (e.g., Kah et al., 2004; Guilbaud et al., 2015), P fixation was likely augmented by vivianite formation in non-sulphidic sediments (Liu et al., 2018; März et al., 2018; Xiong et al., 2019), diminishing the extent of P regeneration to Proterozoic water columns.

3. Estimating Proterozoic seawater phosphate from the record of iron formations

First attempts to reconstruct ancient seawater P levels focussed on iron formations. Indeed, as mentioned above, iron oxides are incredibly efficient at stripping dissolved P *via* coprecipitation and adsorption at the particle surfaces. Therefore, Bjerrum and Canfield (2002) proposed that BIFs can be a passive archive of seawater dissolved P, and suggested that the Archean and most of the Palaeoproterozoic, ferruginous oceans where BIFs deposited witnessed extensive P drawdown from the water column, resulting in a so-called 'P crisis' (Bjerrum and Canfield, 2002).

3.1. Clues from P/Fe ratios in ancient iron formations (IFs)

The assumption is that scavenged P is proportional to seawater phosphate, and therefore the P/Fe ratios in well-preserved BIFs scale linearly with dissolved phosphate concentrations in ancient oceans. Hence, dissolved P concentrations may be calculated back dividing the measured P/Fe ratio by a distribution coefficient (K_D) that describes the partitioning of dissolved phosphate versus phosphate that is adsorbed onto Fe (oxyhydr)oxides. Such covariation between P and Fe contents is beautifully exemplified by recent compilation of P_2O_5 versus Fe_2O_3 data in bulk Archean iron formations (Rego et al., 2023, Fig. 7). Bjerrum and Canfield (2002) used a distribution coefficient (K_D) value ~0.06 μM^{-1}, as found in modern hydrothermal vents where Fe(II) quickly oxidises (Feely et al., 1998), and estimated dissolved [P] <0.6 μM in Archean and early Palaeoproterozoic seawater, ~<25% of modern concentrations.

Caution is required here, however, as the conclusion of low seawater phosphate entirely relies on the estimation of K_D. For instance, Konhauser et al. (2007b) performed coprecipitation experiments to revisit K_D estimates by considering the higher silica contents of Precambrian seawater. Indeed, prior to the rise of silica-biomineralizing organisms such as sponges and their ancestors, marine silica contents would have been comprised between the thresholds imposed by saturation with cristobalite (i.e., 0.67 mM at 40°C) and saturation with amorphous silica (i.e., 2.20 mM) (Maliva et al., 2005), which in both cases surpass the modern ocean dissolved silica concentrations <0.10 mM (Treguer et al., 1995). They found that in the presence of silica, which competes with phosphate on adsorption sites, K_D values significantly diminish to to ~0.011 μM^{-1} and ~0.002 μM^{-1} using cristobalite and amorphous silica saturation conditions, respectively. Therefore, they concluded that dissolved silica in Precambrian seawater greatly impacted on the capacity for ferric (oxyhydro)oxides to withdraw P from solution. Building upon these experimentally derived K_D values, Planavsky et al. (2010) reconstructed the evolution of dissolved P through geologic timescales, using the record of BIFs and iron-rich sediments, and proposed that P concentrations were higher than modern day values throughout the Proterozoic. Yet, another set of experimental data redefined K_D values, not only by considering silica contents, but also using a range of seawater compositions (Jones et al., 2015). Contrasting with previous reports (Konhauser et al., 2007b; Planavsky et al., 2010), the new K_D estimates predict seawater P concentrations <0.15 μM in the early Palaeoproterozoic, at least 18 times lower than the modern ocean (Jones et al., 2015).

Nuancing arguments should be raised here. First, the sensitivity of experimentally derived data, as exemplified above, highlights the risk of strongly diverging interpretations of the rock record. Second, as covered in section 2.3, the sole precipitation of ferric (oxyhydr)oxides under

ferruginous conditions does not reflect the diversity of processes which may withdraw phosphorous from the water column, or, on the opposite, recycling from the sediment during early diagenesis. Even considering that the deposition Fe-rich, chemical sediments such as BIFs was likely to be a major driver for P removal from seawater, ferric (oxyhydr)oxides do not resume the complexity of potential Fe mineral precursors (and therefore the diversity of potential K_D). Indeed, there is a range of precursory phases that may have been involved during the genesis of BIFs and Fe-rich sediments including greenalite (Tosca et al., 2016; Rasmussen et al., 2019; Johnson et al., 2020; B Rasmussen et al., 2021; Guilbaud et al., 2023), green rust (Zegeye et al., 2012; Halevy et al., 2017; Guilbaud et al., 2023), and magnetite (Li et al., 2017), none of which being mutually exclusive (Konhauser et al., 2017).

3.2. Mineralogical considerations

There are still too few experimental studies which address BIF diagenesis, let alone the associated P cycling. In the classical model, ferrihydrite undergoes a range of biogeochemical reactions during early diagenesis that lead to BIF-forming minerals (e.g., Konhauser et al., 2007a). A set of new experiments simulating BIF diagenesis suggests that when organic carbon is present, partial reduction of P-doped ferrihydrite permits the formation of a range of assemblages including siderite, magnetite and vivianite and hematite, with limited remobilisation of P to the porewaters (Schad et al., 2021, Fig. 8). These results are not without caveats: 1) the study lacks to explain chert and Fe(II) silicate genesis (Muhling and Rasmussen, 2020; B Rasmussen et al., 2021); 2) the production of vivianite is only supported by one study (Alibert, 2016), as vivianite is usually absent from BIFs, and so is organic matter. That said, the study also reveals important keys: 1) the produced suite of mineralogical assemblages comprises some major phases that are indeed found in well-preserved BIFs, such as magnetite and siderite; 2) phosphorus recycling seems very limited (<10%), supporting P fixation in the sediment. Note that over geologic timescales, P sink-switches (sections 2.2 and 2.3) likely occurs, favouring the preservation of other minerals such as CFA (Slomp et al., 1996a), and that vivianite formation demands high P loading as a prerequisite (Xiong et al., 2023).

As mentioned above, green rust may have been a common authigenic mineral of Proterozoic oceans (Halevy et al., 2017). Green rust particles can accommodate significant amounts of phosphate adsorbed onto the mineral surfaces (Bocher et al., 2004) or incorporated into the interlayers (Xiong et al., 2023). The transformation of green rust into magnetite and siderite, two of the main constituents of BIFs, during diagenesis and metamorphism has been documented by several studies (e.g., Guilbaud et al., 2013, 2023; Halevy et al., 2017). In particular, the formation of magnetite readily occurs during early diagenesis, at temperatures <100°C (Fig. 9). However,

the fate of phosphorus during these mineralogical transformations is currently unknown and further research is required.

The recent discovery of finely dispersed apatite nanoparticles in Palaeo- and Mesoproterozoic iron formations (Johnson et al., 2020; Birger Rasmussen et al., 2021; Rasmussen et al., 2023) supports CFA formation as a long-term P sink in Fe-rich sediments (Fig. 3). Together with the ubiquitous presence of presumably primary greenalite crystals, dispersed within the cherts of Palaeoproterozoic BIFs (Rasmussen et al., 2019; Muhling and Rasmussen, 2020; B Rasmussen et al., 2021), it has been proposed that Palaeoproterozoic seawater P concentrations were significantly higher than previously thought (Birger Rasmussen et al., 2021; Rasmussen et al., 2023). In particular, Rasmussen et al., (2021) infer that unlike modern hydrothermal systems, where Fe(II) rapidly oxidises and precipitates scavenging P out of the water column, ferruginous Palaeoproterozoic oceans may have allowed, on the contrary, P accumulation in the water column, resulting in its incorporation as disperse apatite nanoparticles in the long-term. This, however, omits the continuous 'Fe wheel' exerted by sinking Fe particles and preventing such accumulation during prolonged periods of ferruginous anoxia (Dellwig et al., 2010; Busigny et al., 2016; Guilbaud et al., 2020). In fact, the presence of nanoparticulate apatite in iron formations rather reflects sediment P fixation from a small reservoir (Jones et al., 2015). High silica contents in seawater favoured the formation of Fe(II) silicates, resulting in CFA being the ultimate P sink, instead of vivianite (Johnson et al., 2020).

The controversy arising from P contents and P mineralogy in IFs leads to my final argument on the limitations inherent to their use as faithful seawater P archives. Despite years of research on the diagenesis of BIFs, they remain extraordinary but also enigmatic geological features. It is yet to be demonstrated that the chemical and mineralogical signatures they carry provide more answers than they raise questions. In contrast to iron-rich chemical sediments, P contents in siliciclastic sediments such as shales offer the significant advantage of a continuous record through the entire geologic timescale. They also consist in sedimentary archives that are way better understood than BIFs, and the biogeochemical mechanisms that occur during their early and burial diagenesis are better constrained. Therefore, we may consider these sediments as a powerful alternative to IFs in order to reconstruct the evolution of the marine dissolved P contents in the Proterozoic.

4. Reconstructing the evolution of the P reservoir through the shale record

4.1. Bulk shale P contents

Recent efforts to build large datasets of P contents in shales were initiated by C. Reinhard and his collaborators (Reinhard et al., 2017, Fig. 10). In their study, they compiled 7,970 new and literature samples from marginal marine settings, focussing on finely grained siliciclastic rocks with Al contents >1 wt%. This filter conveniently excludes sandstones, carbonates and chemical deposits from the data. Reinhard et al. observed relatively low P contents in sediments until ~800-700 Ma, and, contrasting with previous reports (Planavsky et al., 2010), suggested that phosphorus was limiting primary production before 800 Ma, due to efficient P scavenging under ferruginous conditions. This further supports low seawater P concentrations in the Palaeoproterozoic (Bjerrum and Canfield, 2002; Jones et al., 2015). By contrast, sediments younger than ~800-700 Ma yield higher P contents (4 folds higher on average), suggesting a major shift in P cycling and bioavailability, concomitant with shifts in ocean redox chemistry, severe 'snowball Earth' glaciations and the emergence of animal life (Hoffman et al., 1998; Donnadieu et al., 2004; Och and Shields-Zhou, 2012; Planavsky et al., 2014; Lenton et al., 2014).

Augmenting this compilation by another ~>10,000 'shale' samples (with Al contents >2 wt% and excluding phosphorites), Planavsky et al. (2023) drew very similar observations (Fig. 10). Specifically, using change-point methods, they suggest a Tonian (1 to 0,72 a) shift from low-P to high-P regimes, expressed by the 753.3 Ma Visingsö Formation, i.e. before the first Neoproterozoic Sturtian glaciation. Planavsky et al. (2023) hence concluded that the shift in P cycling was unlikely connected to global glacial events, but rather to a shift in ocean redox chemistry, with the likely expansion of oxygenated conditions in the global ocean (Lyons et al., 2014; Planavsky et al., 2014). Note, however, that glaciations themselves being the long-term consequence of continental breakup, increase in seawater phosphate levels may still be coupled with increased LIP weathering during continental breakdown.

The change-point methods on such a large dataset provides a strong support for a shift in the P cycle paradigm around 800 Ma, with low phosphate concentrations in oceans older than ~800 Ma, inferring limited primary production and carbon burial, maintaining low atmospheric pO_2 until the Neoproterozoic Oxygenation Event (Lyons et al., 2014; Planavsky et al., 2014).

The particulate 'Fe wheal' that efficiently scavenges P onto sinking Fe particles (such as green rust) under ferruginous conditions is a popular hypothesis to invoke P-limited productivity and low C_{org} burial during the Proterozoic. In addition, several mechanisms have been invoked to explain P limitations. Laakso and Schrag (2014) suggest that enhanced Fe oxides on continental surfaces, due to low pO_2, may have significantly reduced the flux of P to the oceans throughout the Proterozoic. This, however, needs to be ground-proofed against the break-up of continental masses or the emplacement of large igneous provinces (LIPs), which both may enhance P weathering influxes to the oceans (e.g., Donnadieu et al., 2004; Horton, 2015; Cox et al., 2016;

Alcott et al., 2022). Another scenario is proposed by Kipp and Stüeken (2017), who argue that oxic degradation of organic matter being limited in the Proterozoic, the extent of C_{org} remineralization and P recycling was necessarily diminished (but progressively increased after the GOE). Yet, whilst this is probably true for the global ocean, C_{org} degradation mainly occurred along productive continental margins, which were oxic for most of the Proterozoic (e.g., Poulton and Canfield, 2011). Furthermore, variations in C_{org} preservation (Sperling and Stockey, 2018) observed in concert with varying redox conditions (Guilbaud et al., 2015, 2020) suggest that the efficiency of P recycling also varied throughout the Proterozoic. Finally, Derry (2015), argues that vivianite formation under ferruginous conditions titrated out P from the oceans. Focussing on the high saturation state of the Proterozoic oceans with respect to vivianite (Fig. 11), Derry (2015), suggests that vivianite formation occurs even at low P concentrations. Note that in addition to Fe^{2+}, partial oxidation and precipitation of Fe(III)/Fe(II) phases such as green rust must be considered (Xiong et al., 2023). Experimental and natural data from modern analogues indeed support that vivianite formation may exert a major control on P cycling and bioavailability under eutrophic-mesotrophic ferruginous settings (Cosmidis et al., 2014; O'Connell et al., 2015), as well as in euxinic settings with low sulphate conditions and where an excess of Fe minerals promotes vivianite over pyrite formation (Hsu et al., 2014; März et al., 2018; Xiong et al., 2019; Kubeneck et al., 2021). For lower P contents, however, P removal *via* green rust may dominate over vivianite and the [P] estimates by Derry (2015) likely represent a minimum, consistent with observations from modern, oligotrophic ferruginous lakes (e.g., Crowe et al., 2008; Thompson, 2018).

A striking observation arises from these large compilations and the unanimous picture that emerges from their statistical analysis: despite the redox evolution of the Proterozoic ocean, and the controls exerted by fluctuating redox conditions on the P cycle, the response on bulk shale P contents seems muted for the major part of Earth's history. Why is that? Poulton (2017) noted that bulk P contents in shales only provide a rather restricted understanding of P dynamics, and their interpretation gets limited in several aspects: 1) they do not specifically track bioavailable P, let alone organic P, as a proportion of bulk P may remain inaccessible to organisms (section 2); 2) their use relies on the assumption that bulk shale P contents record a direct reflection of dissolved seawater phosphate, which is unlikely the case. In order to tackle this, Poulton and co-workers (e.g., Thompson et al., 2019; Guilbaud et al., 2020; Bowyer et al., 2020; Alcott et al., 2022) intended to untangle reactive and unreactive P in Proterozoic shales, coupling the partitioning of Fe and P minerals in ancient sediments.

4.2. Coupling the speciation of iron and phosphorus in ancient sediments

Building upon the pioneering SEDEX scheme for modern sediments (Ruttenberg, 1992), and on the Fe speciation method which is used on ancient sediments as a palaeoredox proxy (Poulton and Canfield, 2005), Thompson et al. (2019) addressed the speciation of P in ancient, Fe-rich shales, with a particular focus on the recovery of hematite-bound and magnetite-bound phosphorus. In addition to four of the five operationally defined P pools targeted by the SEDEX method (i.e., P_{Fe1}, P_{auth}, P_{det} and P_{org}), the revised scheme includes extraction steps targeting magnetite-bound phosphorus (P_{mag}) and well-crystalline hematite-bound phosphorus (P_{Fe2}) (Fig. 12).

Particular caution must be taken when applying sequential extractions to ancient sedimentary rocks. Indeed, burial diagenesis and metamorphism affect the crystallinity of certain minerals and may recrystallise others, altering the propensity of some extracting solvents to dissolve the targeted minerals. For instance, the citrate/dithionite/bicarbonate solution used in the SEDEX method to target Fe (oxyhydr)oxides (Ruttenberg, 1992) may not reach the well-crystalline hematite minerals in ancient sedimentary rocks, which are targeted by a more acidic, citrate/dithionite/acetate solution in the Fe speciation method developed by Poulton and Canfield (2005). Another common process which demands caution is the recrystallisation of authigenic P into well-crystalline apatite, which is likely extracted as P_{det}. This was originally observed by the first study applying the SEDEX method on Cambrian sediments (Creveling et al., 2014), whereby ~82% of the P budget was extracted as P_{det} in phosphatic carbonates. In other words, in ancient sedimentary rocks that underwent such recrystallisation, estimations of the reactive P pool are necessarily wrong. However, and luckily, there are still numerous Proterozoic successions where metamorphism was only mild (e.g., sub-greenschist) and where extracted P_{det} truly represents the detrital component, as opposed to recrystallised P_{auth}. To test this, Guilbaud et al. (2020) recommend to check for the absence of correlation between P_{auth} and P_{det}, which would correlate if P_{det} was in large part a product of P_{auth} recrystallisation (Fig. 13A), and the presence of a correlation between P_{det} and a detrital element such as Al or Ti (Fig. 13B). For sediments where these data quality checks are met, one may estimate the proportion of P_{reac} within bulk P contents, of which P_{org} can be remarkably recalcitrant over geologic timescales (Thompson et al., 2019; Guilbaud et al., 2020).

4.2.1. Sediment P recycling at the dawn and the aftermath of the GOE (2.5 to 2.2 Ga)

Coupling Fe and P speciation techniques, Alcott et al. (2022) explore the partitioning of P in ~2.6 to ~2.4 shales and Fe-rich sediments from the Campbellrand and Koegas Subgroups, South Africa. Results demonstrate that, as expected, IFs are efficient scavengers of P under ferruginous conditions, resulting in P fixation in the sediment and low C_{org}/P_{reac} (Fig. 14A). By contrast,

C_{org}/P_{reac} ratios way above the Redfield ratio for oxic, euxinic, but also ferruginous shales indicate that sulphate reduction was sufficient to promote intense P remobilisation during early diagenesis. In their model, Alcott et al. (2022) suggest that increasing sulphate levels prior to the GOE enhanced for the first time in Earth's history the regeneration of significant dissolved P to the water column which, possibly combined with higher P influxes due to the LIPs weathering, resulted in a positive feedback on primary production, C_{org} burial, and oxygen outgassing, leading to the GOE.

During the GOE, the transient cessation in BIF deposition agrees with the expansion of euxinic continental margins (Fig. 2), with nevertheless low sulphate levels (Kah et al., 2004). This may have resulted in the precipitation of recycled P as vivianite (e.g., Xiong et al., 2019) or CFA (e.g., Birger Rasmussen et al., 2021) in neighbouring ferruginous settings, or in its accumulation as dissolved phosphate in eutrophic and euxinic water masses. At the end of the GOE, during the Lomagundi Event, accumulated P may have titrated out of seawater, leading to the first economical phosphorite deposits (Fig. 1, Bekker and Holland, 2012).

4.2.2. Maintaining low, but fluctuating O_2 levels through the Earth's middle age (~1.8 to 0.8 Ga)

The study of late Palaeo- and Mesoproterozoic shales deposited under euxinic conditions also shows elevated C_{org}/P_{reac} ratios, surpassing the Redfield ratio (Guilbaud et al., 2020, Fig. 14B). This further gives support for P recycling to the water column due to the establishment of euxinic conditions along productive continental margins by ~1.8 Ga (Poulton et al., 2010), and the synchronous cessation of BIF deposition. However, P recycling may have been less severe than during the GOE, since P-doped, Fe-rich sediments as existed in the early Palaeoproterozoic would have been exhausted by extensive sulphide recycling (Alcott et al., 2022). Studying the phase partitioning of P in oxic and ferruginous sediments from the ~1.8-1.4 Ga Yanshan Basin, North China, Doyle et al. (2018) showed that reactive P was effectively removed from a P-limited basin and accumulated in the sediment. Together, combined Fe and P speciation results may explain the O_2 recovery and stabilisation directly after the GOE-Lomagundi suite of events (Poulton et al., 2021), whereby less extensive P recycling may eventually result in less C_{org} burial and less atmospheric O_2 production. The extent of P recycling may have further been nuanced by sedimentary sinks such as vivianite (Derry, 2015) and CFA (Johnson et al., 2020), limiting the formation of phosphorite deposits during that time interval (Derry, 2015).

In sharp contrast with this scenario, euxinic conditions nearly disappear at ~1 Ga, presumably because of decreased Fe influxes from supercontinent Rodinia (Guilbaud et al., 2015; Sperling et al., 2015, Fig. 2). Analysing the partitioning of P in a ~1-0.9 Ga ferruginous basin of the North China craton, Guilbaud et al. (2020) showed that P_{det} constitutes a major part of the already

diminished P flux to the oceans, suggesting that reactive P was significantly retained on the continents, due to the mobility of Fe particles on Rodinia. This agrees, at least for the early Neoproterozoic, with the continental P retention mechanism proposed by Laakso and Schrag (2014). Note that terrestrial, lacustrine environments of the ~1 Ga Torridon Group, Scotland, comprise significant P deposits (Fig. 15) which preserve early terrestrial eukaryotes (e.g., Battison and Brasier, 2012; Brasier et al., 2017; Wacey et al., 2017). Current mechanism to explain lacustrine phosphogenisis invokes redox-controlled P accumulation at the sediment-water interface and the precipitation of microcrystalline apatite when supersaturation conditions are reached (Battison and Brasier, 2012).

Guilbaud et al. (2020) suggest that extensive P drawdown by sinking green rust particles (Xiong et al., 2023) in early Neoproterozoic oceans, and its fixation in the sediment as P_{reac}, maintained low C_{org} burial under an oligotrophic ocean, and low atmospheric O_2 conditions. This is further supported by C_{org}/P_{reac} ratios below the Redfiled ratio, as opposed to previous Palaeo- and Mesoproterozoic formations (Fig. 14B). In the model, Guilbaud et al. (2020) suggest that in order to maintain an oxidised atmosphere during that period of time, seawater [P] concentrations must have been >0.55 μM, based on the $pO_2/[PO_4]$ ratio required to keep the atmosphere at ~0.1 PAL (Planavsky et al., 2014; Lenton and Daines, 2017).

4.2.3. Late Neoproterozoic dynamics

The later Neoproterozoic (~0.8 to 0.542 Ga) is characterized by a net increase in phosphorite deposition and bulk shale P contents (Holland, 2005; Reinhard et al., 2017; Planavsky et al., 2023). Current models to explain this increase in sedimentary P invoke the breakup of Rodinia and the weathering of LIPs, eventually leading to the severe Neoproterozoic glaciations (Donnadieu et al., 2004; Horton, 2015; Cox et al., 2016). By contrast, others invoke redox-related mechanisms, such as the intensification of sulphide-induced P recycling from the sediments due to increasing seawater sulphate concentrations (Laakso et al., 2020), or O_2-induced C_{org} remineralisation (Kipp and Stüeken, 2017), without additional weathering fluxes. Some proposed that increased P levels in the late Neoproterozoic may have contributed to the fundamental switch from a cyanobacterial- to a eukaryotic-dominated biomass at the end of the first Neoproterozoic glaciation, and the subsequent radiation of metazoans (Brocks et al., 2017).

However, questioning the idea of increased seawater P levels, studies on the partitioning of P in several Ediacaran (635 to 541 Ma) successions from Russia, Australia, Western Canada, Newfoundland and Namibia suggest P depletion or limited, local enrichments compared to the average shale (Doyle, 2018; Bowyer et al., 2020). Further, when observed, P enrichments are found in association with increased detrital inputs (P_{det}) rather than authigenic phases (Doyle, 2018), which bulk shale P contents do not permit to address (Poulton, 2017). As mentioned above,

the late Neoproterozoic is characterized by shifts in redoxcline depth, with conditions oscillating from oxic to ferruginous, until the development of modern-like oxygen minimum zones in a fully ventilated ocean (Canfield et al., 2007; Wood et al., 2015; Tostevin et al., 2016, 2019; Guilbaud et al., 2018). The role played by phosphorus in this redox context may be inferred by these P speciation data. Indeed, Bowyer et al. (2020) propose that the long term decrease in available P under oxic and ferruginous water columns may have led to the progressive ventilation of the global ocean, and that persistently oxygenated shallow waters with P fixation in the sediment may have favoured the ideal conditions for complex life to expand and diversify. On similar lines of thoughts, models suggest that the generation of larger, faster-sinking organic pellets would have deepened oxygen demand from shallow waters to deeper waters, limited P recycling to the water column and sustained oxic conditions in the Ediacaran (Butterfield, 2009; Lenton et al., 2014).

Recently, Dodd et al. (2023) further supported the scenario of decreased nutrients in the Ediacaran, using the newly developed carbonate-associated phosphorus proxy (CAP) as a direct estimate for seawater phosphate (Dodd et al., 2021). They find a first increase in seawater P, presumably due to enhanced seawater sulphate inputs (Laakso et al., 2020), potentially leading to a negative feedback on primary productivity and O_2 production. In turn, higher O_2 would have limited the extent of anoxia, which they observe using 'stable' uranium isotopes ($\delta^{238}U$) as a palaeoredox proxy. Lower extent of ocean anoxia, and therefore lesser P recycling, would have resulted in a further drawdown in the marine P reservoir (Dodd et al., 2023). A lower P reservoir would have promoted sustained oxic conditions in the water column, and the stabilisation of the P-O_2 cycle in the terminal Ediacaran (Doyle, 2018; Bowyer et al., 2020). The advent of motile macroscopic animals ~565 Ma (Liu et al., 2010), which oxidised the upper sediments through bioturbations, may have further decreased P release to the water column and stabilised the P-O_2 cycle (Boyle et al., 2014).

Dodd et al. (2023) highlight that CAP values are similar under both maximal and minimal oceanic anoxia, implying that P recycling was muted during extensive seafloor anoxia. They propose that this decoupling of CAP values and $\delta^{238}U$ reflects decoupling in the P-O_2 cycle, divorcing from the modern day where such coupling exists. Building upon this observation, Dodd et al. (2023) suggest that such decoupling may have been active throughout most of the Precambrian, questioning the paradigm of P-O_2 coupling throughout Earth's history. This is an appealing theory, as direct evidence for P-O_2 coupling in the Precambrian is not always trivial. In fact, as widely seen throughout sections 3 and 4, Precambrian P-O_2 coupling is often a presupposed assumption invoked to interpret the geochemical record. This assertion will therefore have to be ground-proofed on other Proterozoic successions, and the following warrants must be considered: 1) if CAP and $\delta^{238}U$ are simultaneously recorded in ancient

carbonates, can the redox signal and the nutrient response be anything else but decoupled? In other words, there must be a lag time to be considered, and so on geologic timescales; 2) in the modern day the response in P recycling to the extent of anoxia is commonly observed in euxinic environments, whilst oligotrophic, ferruginous systems (e.g., Lake Towuti) are probably better analogues for the Ediacaran period; 3) Dodd et al. (2023) invoke invariable C_{org}/P_{tot} under a range of redox conditions in the Ediacaran to confirm this decoupling, which is biased by the large proportion of unreactive P_{det} within total P (Doyle, 2018; Bowyer et al., 2020).

5. Evolution of the C/P ratio through time

Whilst this has become common practice to consider the C/P ratio in deep times (Fig. 14), one should also bear in mind that it directly depends on the preservation of organic matter through time, which itself is affected by oxidation processes, loss *via* oil transport, and sampling bias. This considered, statistical trends in TOC contents can be observed (e.g., Sperling and Stockey, 2018), and therefore The C/P ratios may provide additional insights on the extent of P recycling to the Proterozoic water column. As covered in section 2, sulphide-induced P regeneration from the sediment may be snapshotted by sedimentary C/P (Fig. 4). Utilizing the dataset collected by Reinhard et al. (2017) and augmented by several Proterozoic studies (Guilbaud et al., 2020; Bowyer et al., 2020; Alcott et al., 2022), I now explore the C_{org}/P_{tot} ratio throughout Earth history (Fig. 16).

Reinhard et al. (2017) propose that because of efficient P scavenging under ferruginous conditions in pre-800 Ma sediments, strong P limitations on primary production may have resulted in elevated C/P ratios (~300:1 to 400:1), divorcing from the canonical Redfield ratio of 106:1. Indeed, the data show that C/P can be elevated in the Proterozoic, at least until ~1.1 Ga. Interestingly, for the Phanerozoic, median C/P values point precisely towards the Redfield ratio, whereas mean C/P values are higher, highlighting the variability due to P recycling by sulphide (Table 2). By contrast, mean and median C/P values for the Proterozoic strongly diverge (Table 2), making the assumption of Reinhard et al. (2017) difficult to address. I suggest that this can be circumvented by exploring the C_{org}/P_{org} ratio, as opposed to C_{org}/P_{tot}, in shales deposited under oxic and ferruginous conditions, and where sulphide-induced P recycling was kept to a minimal.

The ~1-0.9 Ga Huainan Basin, North China, was interpreted as an oligotrophic basin where sediments deposited under oxic and ferruginous conditions with vanishingly low sulphide contents (Guilbaud et al., 2015, 2020). Similarly, late Ediacaran shelf sediments from the Nama Group, Namibia, record low P availability in oxic and ferruginous sediments where sulphide production is virtually absent (Bowyer et al., 2020). Both locations therefore provide the ideal conditions to test the hypothesis that nutrient uptake by organisms under Proterozoic P-limiting

conditions strongly departed from the canonical Redfield ratio (Reinhard et al., 2017). The data, nevertheless, shows that C_{org}/P_{org} ratios remarkably cluster around the Redfield line of 106:1, as in the modern world (Fig. 17A). This certainly does not imply that the Redfield ratio did not evolved throughout the Proterozoic; yet the preliminary data that are available to address that specific question seem to suggest that modern-like nutrient uptake by organisms already operated in the Neoproterozoic. Ferruginous and oxic sediments with low sulphide production from the ~1.6 Ga Yanshan Basin (Doyle, 2018), by contrast, show some data departing from the Redfield ratio, suggesting that, perhaps, phosphorus uptake by organisms may have diverged then (Fig. 17B).

There is a tight relationship between nutrient concentrations in the deep ocean today, which closely match the Redfield ratio measured in marine phytoplankton, and dissolved oxygen concentrations which are just sufficient to respire C_{org} (Lenton and Watson, 2000). In other words, the antiquity of the Redfield ratio in sediments may track back to the establishment of modern-like dynamics, whereby eukaryotic algae thrive in an oxic photic zone, with a P reservoir limited by P fixation in the sediment. Considering our current understanding of the redox dynamics in the Neoproterozoic, characterised by a protracted deepening of the redoxcline with ferruginous conditions in the deeper waters, Redfield-matching C_{org}/P_{org} ratios by ~1 Ga may support an early Neoproterozoic establishment of such conditions. Alternatively, they could well reflect the switch to eukaryotic-dominated organic matter, as the P uptake ratio by ancient prokaryotes is currently unknown.

6. Summary and perspectives

Attempts to reconstruct phosphorus availability through the Proterozoic are important in order to test hypotheses such as nutrient or trace metal limitations on the evolution of life, and particularly eukaryotes (Anbar and Knoll, 2002; Planavsky et al., 2010). Fig. 18 shows the reconstruction of recycled phosphorus through time (Kipp and Stüeken, 2017), with proposed associated dissolved P contents in the deep ocean. The difference between the two arises from the trapping of recycled P under dominantly ferruginous water columns. In the early Palaeoproterozoic, before the GOE, intense P drawdown onto Fe particles may have restricted deep ocean P concentrations to <0.15 μM (Jones et al., 2015), with only limited recycling (Schad et al., 2021). Increasing sulphate reduction and the establishment of transient euxinic water masses along continental margins ~2.4-1.9 Ga likely enhanced the flux of recycled P to the water column (Kipp and Stüeken, 2017; Alcott et al., 2022), and yet the global ferruginous ocean may still have been phosphate depleted, due to extensive Fe-associated P drawdown. During the following 1.8-1.0 Ga period, which records fossil evidence for ancestral eukaryotic cells and their

early evolution (Butterfield, 2000; Knoll et al., 2006; Javaux, 2011; Zhu et al., 2016), such recycling may have been less intense, but still active (Guilbaud et al., 2020), due to common euxinic conditions in shallow waters (Poulton and Canfield, 2011; Guilbaud et al., 2015; Sperling et al., 2015). P recycling was likely nuanced by adsorption/coprecipitation onto Fe minerals such as green rust and vivianite (Xiong et al., 2019), and P concentrations in equilibrium with vivianite suggest that seawater [P] may have been as low as 0.2 μM (Derry, 2015). In the early Neoproterozoic, the near disappearance of euxinic water masses along continental margins (Sperling et al., 2015) promoted P fixation in the sediment, with lower estimates for deep ocean [P] ~0.55 μM (Guilbaud et al., 2020), in order to keep pO_2 ~0.1 PAL (Planavsky et al., 2014). However, the observation that C_{org}/P_{org} matched the canonical Redfield ratio may imply that phosphate levels were higher, perhaps as in the modern ocean (~2.3 μM). Late Ediacaran studies point towards a low P reservoir under protracted oxygenating conditions (Bowyer et al., 2020; Dodd et al., 2023), which would have stabilised the ventilation of the full ocean and the P-O_2 cycles in the long term, paving the way for early metazoans at the surface of sediments where nutrient fixation occurred under oxic water columns. The long term Neoproterozoic drawdown of P from the water column, together with sulphide-rich conditions being limited to the sediment, may explain the general increase in bulk shale P contents and in phosphorite deposits (Reinhard et al., 2017; Planavsky et al., 2023).

The brief summary depicted above is undoubtedly not without caveat, and I am sure it will continue evolving along with ongoing discoveries. The take-home message is certainly that over the last 20 years or so, reconstructions of the phosphorus cycle in the Proterozoic have been notoriously difficult to make. The observation of the modern world, and in particular the peculiar anoxic environments which can be (sometimes misleadingly) considered as analogues to the deep past, has greatly contributed to this research. Yet, the actualistic approach also carries its range of presupposed concepts, such as the coupled P-O_2 cycle to cite only one, which may or may not be relevant to the early Earth. Experimental work has proven to provide extremely valuable insights. It is true that experimental studies tend to focus on simplified systems with condition limits that are far away from the real world. Yet, it is by doing so (and only so!) that one may isolate and quantify specifically targeted mechanisms, which otherwise in nature occur in concert with a range of others. Further research providing more experimental data should help refine models. In particular, experiments accounting for the range of complex mineralogies relevant to the Proterozoic ocean, and which all can coexist. Finally, research on the antiquity of the Redfield ratio, and tracing its occurrence as C_{org}/P_{org} in older, Proterozoic sediments which have undergone limited C_{org} oxidation, might help us understand the evolution of the C-P-O cycles and the metabolism of ancient prokaryotic and eukaryotic organisms.

Acknowledgments

I thank R. Craviotto-Arnau for proofreading the original text and ANR-21-CE49-0007-01 for financial support. I am thankful to many of my collaborators over the years, with whom I shared scientific discussions on the topic of phosphorus in the deep time, which helped construct the narrative presented here, as well as Sasha Turchyn and an anonymous reviewer.

References

Alcott L. J., Mills B. J. and Poulton S. W. (2019) Stepwise Earth oxygenation is an inherent property of global biogeochemical cycling. *Science* **366**, 1333–1337.

Alcott L. J., Mills B. J. W., Bekker A. and Poulton S. W. (2022) Earth's Great Oxidation Event facilitated by the rise of sedimentary phosphorus recycling. *Nature Geoscience* **15**, 210–215.

Alibert C. (2016) Rare earth elements in Hamersley BIF minerals. *Geochimica et Cosmochimica Acta* **184**, 311–328.

Anbar A. D., Duan Y., Lyons T. W., Arnold G. L., Kendall B., Creaser R. A., Kaufman A. J., Gordon G. W., Scott C., Garvin J. and Buick R. (2007) A Whiff of Oxygen Before the Great Oxidation Event? *Science* **317**, 1903–1906.

Anbar A. D. and Knoll A. (2002) Proterozoic ocean chemistry and evolution: a bioinorganic bridge? *Science* **297**, 1137–1142.

Anderson L. A. and Sarmiento J. L. (1994) Redfield ratios of remineralization determined by nutrient data analysis. *Global biogeochemical cycles* **8**, 65–80.

Anderson L., Delaney M. and Faul K. (2001) Carbon to phosphorus ratios in sediments: Implications for nutrient cycling. *Global Biogeochemical Cycles* **15**, 65–79.

Battison L. and Brasier M. D. (2012) Remarkably preserved prokaryote and eukaryote microfossils within 1Ga-old lake phosphates of the Torridon Group, NW Scotland. *Precambrian Research* **196**, 204–217.

Bauer K. W., Byrne J. M., Kenward P., Simister R., Michiels C., Friese A., Vuillemin A., Henny C., Nomosatryo S. and Kallmeyer J. (2020) Magnetite biomineralization in ferruginous waters and early Earth evolution. *Earth and Planetary Science Letters* **549**, 116495.

Bekker A. and Holland H. (2012) Oxygen overshoot and recovery during the early Paleoproterozoic. *Earth and Planetary Science Letters* **317**, 295–304.

Bekker A., Holland H. D., Wang P. L., Rumble D. I., Stein H. J., Hannah J. L., Coetzee L. L. and Beukes N. J. (2004) Dating the rise of atmospheric oxygen. *Nature* **427**, 117–120.

Berner R. A. (1989) Biogeochemical cycles of carbon and sulfur and their effect on atmospheric oxygen over Phanerozoic time. *Global and Planetary Change* **1**, 97–122.

Berner R. A. and Canfield D. E. (1989) A new model for atmospheric oxygen over Phanerozoic time. *American journal of Science* **289**, 333–361.

Bjerrum C. J. and Canfield D. E. (2002) Ocean productivity before about 1.9 Gyr ago limited by phosphorus adsorption onto iron oxides. *Nature* **417**, 159.

Björkman K. M. and Karl D. M. (2003) Bioavailability of dissolved organic phosphorus in the euphotic zone at Station ALOHA, North Pacific Subtropical Gyre. *Limnology and Oceanography* **48**, 1049–1057.

Bocher F., Géhin A., Ruby C., Ghanbaja J., Abdelmoula M. and Génin J.-M. R. (2004) Coprecipitation of Fe(II–III) hydroxycarbonate green rust stabilised by phosphate adsorption. *Solid State Sciences* **6**, 117–124.

Bowyer F. T., Shore A. J., Wood R. A., Alcott L. J., Thomas A. L., Butler I. B., Curtis A., Hainanan S., Curtis-Walcott S., Penny A. M. and Poulton S. W. (2020) Regional nutrient decrease drove redox stabilisation and metazoan diversification in the late Ediacaran Nama Group, Namibia. *Scientific Reports* **10**, 2240.

Boyle R. A., Dahl T. W., Dale A. W., Shields-Zhou G. A., Zhu M., Brasier M. D., Canfield D. E. and Lenton T. M. (2014) Stabilization of the coupled oxygen and phosphorus cycles by the evolution of bioturbation. *Nature Geosci* **advance online publication**.

Brady M. P., Tostevin R. and Tosca N. J. (2022) Marine phosphate availability and the chemical origins of life on Earth. *Nature Communications* **13**, 5162.

Brasier A., Culwick T., Battison L., Callow R. and Brasier M. (2017) Evaluating evidence from the Torridonian Supergroup (Scotland, UK) for eukaryotic life on land in the Proterozoic. *Geological Society, London, Special Publications* **448**, 121–144.

Brasier M. D., Green O. R., Jephcoat A. P., Kleppe A. K., Van Kranendonk M. J., Lindsay J. F., Steele A. and Grassineau N. V. (2002) Questioning the evidence for Earth's oldest fossils. *Nature* **416**, 76–81.

Brocks J. J., Jarrett A. J., Sirantoine E., Hallmann C., Hoshino Y. and Liyanage T. (2017) The rise of algae in Cryogenian oceans and the emergence of animals. *Nature* **548**, 578.

Busigny V., Jézéquel D., Cosmidis J., Viollier E., Benzerara K., Planavsky N. J., Albéric P., Lebeau O., Sarazin G. and Michard G. (2016) The Iron Wheel in Lac Pavin: interaction with phosphorus cycle. *Lake Pavin: History, geology, biogeochemistry, and sedimentology of a deep meromictic maar lake*, 205–220.

Butterfield N. J. (2000) Bangiomorpha pubescens n. gen., n. sp.: implications for the evolution of sex, multicellularity, and the Mesoproterozoic/Neoproterozoic radiation of eukaryotes. *Paleobiology* **26**, 386–404.

Butterfield N. J. (2009) Oxygen, animals and oceanic ventilation: an alternative view. *Geobiology* **7**, 1–7.

Canfield D. E. (1998) A new model for Proterozoic ocean chemistry. *Nature* **396**, 450–453.

Canfield D. E., Poulton S. W., Knoll A. H., Narbonne G. M., Ross G., Goldberg T. and Strauss H. (2008) Ferruginous Conditions Dominated Later Neoproterozoic Deep-Water Chemistry. *Science* **321**, 949–952.

Canfield D. E., Poulton S. W. and Narbonne G. M. (2007) Late-Neoproterozoic Deep-Ocean Oxygenation and the Rise of Animal Life. *Science* **315**, 92–95.

Canfield D. E., Raiswell R. and Bottrell S. H. (1992) The reactivity of sedimentary iron minerals toward sulfide. *American Journal of Science* **292**, 659–683.

Canfield D. and Thamdrup B. (2009) Towards a consistent classification scheme for geochemical environments, or, why we wish the term 'suboxic'would go away. *Geobiology* **7**, 385–392.

Cosmidis J., Benzerara K., Morin G., Busigny V., Lebeau O., Jezequel D., Noel V., Dublet G. and Othmane G. (2014) Biomineralization of iron-phosphates in the water column of Lake Pavin (Massif Central, France). *Geochimica et Cosmochimica Acta* **126**, 78–96.

Cox G. M., Halverson G. P., Stevenson R. K., Vokaty M., Poirier A., Kunzmann M., Li Z.-X., Denyszyn S. W., Strauss J. V. and Macdonald F. A. (2016) Continental flood basalt weathering as a trigger for Neoproterozoic Snowball Earth. *Earth and Planetary Science Letters* **446**, 89–99.

Creveling J. R., Johnston D. T., Poulton S. W., Kotrc B., März C., Schrag D. P. and Knoll A. H. (2014) Phosphorus sources for phosphatic Cambrian carbonates. *Geological Society of America Bulletin* **126**, 145–163.

Crowe S. A., Jones C., Katsev S., Magen C., O'Neill A. H., Sturm A., Canfield D. E., Haffner G. D., Mucci A. and Sundby B. (2008) Photoferrotrophs thrive in an Archean Ocean analogue. *Proceedings of the National Academy of Sciences* **105**, 15938–15943.

Dahl T. W., Canfield D. E., Rosing M. T., Frei R. E., Gordon G. W., Knoll A. H. and Anbar A. D. (2011) Molybdenum evidence for expansive sulfidic water masses in~ 750Ma oceans. *Earth and Planetary Science Letters* **311**, 264–274.

Delaney M. (1998) Phosphorus accumulation in marine sediments and the oceanic phosphorus cycle. *Global Biogeochemical Cycles* **12**, 563–572.

Dellwig O., Leipe T., März C., Glockzin M., Pollehne F., Schnetger B., Yakushev E. V., Böttcher M. E. and Brumsack H.-J. (2010) A new particulate Mn–Fe–P-shuttle at the redoxcline of anoxic basins. *Geochimica et Cosmochimica Acta* **74**, 7100–7115.

Derry L. A. (2015) Causes and consequences of mid-Proterozoic anoxia. *Geophysical Research Letters* **42**, 8538–8546.

Dijkstra N., Hagens M., Egger M. and Slomp C. P. (2018a) Post-depositional formation of vivianite-type minerals alters sediment phosphorus records. *Biogeosciences* **15**, 861–883.

Dijkstra N., Kraal P., Kuypers M. M., Schnetger B. and Slomp C. P. (2014) Are iron-phosphate minerals a sink for phosphorus in anoxic Black Sea sediments? *PloS one* **9**, e101139.

Dijkstra N., Kraal P., Séguret M., Flores M., Gonzalez S., Rijkenberg M. J. and Slomp C. (2018b) Phosphorus dynamics in and below the redoxcline in the Black Sea and implications for phosphorus burial. *Geochimica et Cosmochimica Acta* **222**, 685–703.

Dijkstra N., Slomp C. P. and Behrends T. (2016) Vivianite is a key sink for phosphorus in sediments of the Landsort Deep, an intermittently anoxic deep basin in the Baltic Sea. *Chemical Geology* **438**, 58–72.

Dodd M. S., Shi W., Li C., Zhang Z., Cheng M., Gu H., Hardisty D. S., Loyd S. J., Wallace M. W. and vS. Hood A. (2023) Uncovering the Ediacaran phosphorus cycle. *Nature*, 1–7.

Dodd M. S., Zhang Z., Li C., Algeo T. J., Lyons T. W., Hardisty D. S., Loyd S. J., Meyer D. L., Gill B. C., Shi W. and Wang W. (2021) Development of carbonate-associated phosphate (CAP) as a proxy for reconstructing ancient ocean phosphate levels. *Geochimica et Cosmochimica Acta* **301**, 48–69.

Donnadieu Y., Goddéris Y., Ramstein G., Nédélec A. and Meert J. (2004) A 'snowball Earth' climate triggered by continental break-up through changes in runoff. *Nature* **428**, 303–306.

Dos Santos Afonso M. and Stumm W. (1992) Reductive dissolution of iron (III)(hydr) oxides by hydrogen sulfide. *Langmuir* **8**, 1671–1675.

Doyle K. A. (2018) The chemical evolution of the Proterozoic biosphere.

Doyle K. A., Poulton S. W., Newton R. J., Podkovyrov V. N. and Bekker A. (2018) Shallow water anoxia in the Mesoproterozoic ocean: Evidence from the Bashkir Meganticlinorium, Southern Urals. *Precambrian Research* **317**, 196–210.

Egger M., Jilbert T., Behrends T., Rivard C. and Slomp C. P. (2015) Vivianite is a major sink for phosphorus in methanogenic coastal surface sediments. *Geochimica et Cosmochimica Acta* **169**, 217–235.

Farquhar J., Bao H. and Thiemens M. (2000) Atmospheric Influence of Earth's Earliest Sulfur Cycle. *Science* **289**, 756–758.

Feely R. A., Trefry J. H., Lebon G. T. and German C. R. (1998) The relationship between P/Fe and V/Fe ratios in hydrothermal precipitates and dissolved phosphate in seawater. *Geophysical Research Letters* **25**, 2253–2256.

Filippelli G. M. and Delaney M. L. (1996) Phosphorus geochemistry of equatorial Pacific sediments. *Geochimica et Cosmochimica Acta* **60**, 1479–1495.

Froelich P. N., Klinkhammer G. P., Bender M. L., Luedtke N. A., Heath G. R., Cullen D., Dauphin P., Hammond D., Hartman B. and Maynard V. (1979) Early oxidation of organic matter in pelagic sediments of the eastern equatorial Atlantic: suboxic diagenesis. *Geochimica et Cosmochimica Acta* **43**, 1075–1090.

Frohlich P., Bender M., Luedtke N., Heath G. and DeVries T. (1982) Marine phosphorus cycle. *Am. J. Sci.;(United States)* **282**.

Goldman J. C., McCarthy J. J. and Peavey D. G. (1979) Growth rate influence on the chemical composition of phytoplankton in oceanic waters. *Nature* **279**, 210–215.

Guilbaud R., Boulard E., Baptiste B., Delbes L., Menjot L. and Guarnelli Y. (2023) Burial of Fe bearing precursors to 'chemical sediments' in the deep past. In Goldschmidt 2023 Conference. GOLDSCHMIDT.

Guilbaud R., Poulton S. W., Butterfield N. J., Zhu M. and Shields-Zhou G. A. (2015) A global transition to ferruginous conditions in the early Neoproterozoic oceans. *Nature Geoscience* **8**, 466–470.

Guilbaud R., Poulton S. W., Thompson J., Husband K. F., Zhu M., Zhou Y., Shields G. A. and Lenton T. M. (2020) Phosphorus-limited conditions in the early Neoproterozoic ocean maintained low levels of atmospheric oxygen. *Nature Geoscience* **13**, 296–301.

Guilbaud R., Slater B. J., Poulton S. W., Harvey T. H. P., Brocks J. J., Nettersheim B. J. and Butterfield N. J. (2018) Oxygen minimum zones in the early Cambrian ocean. *Geochemical Perspectives Letters* **6**, 33–38.

Guilbaud R., White M. L. and Poulton S. W. (2013) Surface charge and growth of sulphate and carbonate green rust in aqueous media. *Geochimica et Cosmochimica Acta* **108**, 141–153.

Halevy I., Alesker M., Schuster E., Popovitz-Biro R. and Feldman Y. (2017) A key role for green rust in the Precambrian oceans and the genesis of iron formations. *Nature Geoscience* **10**, 135–139.

Hoffman P. F., Kaufman A. J., Halverson G. P. and Schrag D. P. (1998) A Neoproterozoic Snowball Earth. *Science* **281**, 1342–1346.

Holland H. D. (2005) 100th anniversary special paper: sedimentary mineral deposits and the evolution of earth's near-surface environments. *Economic Geology* **100**, 1489–1509.

Horton F. (2015) Did phosphorus derived from the weathering of large igneous provinces fertilize the Neoproterozoic ocean? *Geochemistry, Geophysics, Geosystems* **16**, 1723–1738.

Hsu T.-W., Jiang W.-T. and Wang Y. (2014) Authigenesis of vivianite as influenced by methane-induced sulfidization in cold-seep sediments off southwestern Taiwan. *Journal of Asian Earth Sciences* **89**, 88–97.

Ingall E. D., Bustin R. and Van Cappellen P. (1993) Influence of water column anoxia on the burial and preservation of carbon and phosphorus in marine shales. *Geochimica et Cosmochimica Acta* **57**, 303–316.

Ingall E. D. and Van Cappellen P. (1990) Relation between sedimentation rate and burial of organic phosphorus and organic carbon in marine sediments. *Geochimica et Cosmochimica Acta* **54**, 373–386.

Ingall E. and Jahnke R. (1997) Influence of water-column anoxia on the elemental fractionation of carbon and phosphorus during sediment diagenesis. *Marine Geology* **139**, 219–229.

Isley A. E. and Abbott D. H. (1999) Plume-related mafic volcanism and the deposition of banded iron formation. *J. Geophys. Res.* **104**, 15461–15477.

Jarvis I., Burnett W., Nathan Y., Almbaydin F., Attia A., Castro L., Flicoteaux R., Hilmy M. E., Husain V. and Qutawnah A. (1994) Phosphorite geochemistry: state-of-the-art and environmental concerns. *Eclogae Geologicae Helvetiae* **87**, 643–700.

Javaux E. (2011) Early eukaryotes in Precambrian oceans. *Origins and evolution of life: An astrobiological perspective* **6**, 414.

Johnson B. R., Tostevin R., Gopon P., Wells J., Robinson S. A. and Tosca N. J. (2020) Phosphorus burial in ferruginous SiO2-rich Mesoproterozoic sediments. *Geology* **48**, 92–96.

Johnston D. T., Poulton S. W., Dehler C., Porter S., Husson J., Canfield D. E. and Knoll A. H. (2010) An emerging picture of Neoproterozoic ocean chemistry: Insights from the Chuar Group, Grand Canyon, USA. *Earth and Planetary Science Letters* **290**, 64–73.

Jones C., Nomosatryo S., Crowe S. A., Bjerrum C. J. and Canfield D. E. (2015) Iron oxides, divalent cations, silica, and the early earth phosphorus crisis. *Geology* **43**, 135–138.

Kah L. C., Lyons T. W. and Frank T. D. (2004) Low marine sulphate and protracted oxygenation of the Proterozoic biosphere. *Nature* **431**, 834–838.

Kappler A., Pasquero C., Konhauser K. O. and Newman D. K. (2005) Deposition of banded iron formations by anoxygenic phototrophic Fe (II)-oxidizing bacteria. *Geology* **33**, 865–868.

Karl D. M. and Björkman K. M. (2015) Chapter 5 - Dynamics of Dissolved Organic Phosphorus. In *Biogeochemistry of Marine Dissolved Organic Matter (Second Edition)* (eds. D. A. Hansell and C. A. Carlson). Academic Press, Boston. pp. 233–334.

Kaufman A. J., Johnston D. T., Farquhar J., Masterson A. L., Lyons T. W., Bates S., Anbar A. D., Arnold G. L., Garvin J. and Buick R. (2007) Late Archean Biospheric Oxygenation and Atmospheric Evolution. *Science* **317**, 1900–1903.

Kendall B., Reinhard C. T., Lyons T. W., Kaufman A. J., Poulton S. W. and Anbar A. D. (2010) Pervasive oxygenation along late Archaean ocean margins. *Nature Geosci* **3**, 647–652.

Kipp M. A. and Stüeken E. E. (2017) Biomass recycling and Earth's early phosphorus cycle. *Science advances* **3**, eaao4795.

Knoll A. H. and Carroll S. B. (1999) Early Animal Evolution: Emerging Views from Comparative Biology and Geology. *Science* **284**, 2129–2137.

Knoll A. H., Javaux E. J., Hewitt D. and Cohen P. (2006) Eukaryotic organisms in Proterozoic oceans. *Philosophical Transactions of the Royal Society B: Biological Sciences* **361**, 1023–1038.

Konhauser K. O., Amskold L., Lalonde S. V., Posth N. R., Kappler A. and Anbar A. (2007a) Decoupling photochemical Fe (II) oxidation from shallow-water BIF deposition. *Earth and Planetary Science Letters* **258**, 87–100.

Konhauser K. O., Lalonde S. V., Amskold L. and Holland H. D. (2007b) Was there really an Archean phosphate crisis? *Science* **315**, 1234–1234.

Konhauser K. O., Planavsky N., Hardisty D., Robbins L., Warchola T., Haugaard R., Lalonde S., Partin C., Oonk P. and Tsikos H. (2017) Iron formations: A global record of Neoarchaean to Palaeoproterozoic environmental history. *Earth-Science Reviews* **172**, 140–177.

Kraal P., Dijkstra N., Behrends T. and Slomp C. P. (2017) Phosphorus burial in sediments of the sulfidic deep Black Sea: Key roles for adsorption by calcium carbonate and apatite authigenesis. *Geochimica et Cosmochimica Acta* **204**, 140–158.

Krom M. D. and Berner R. A. (1980) Adsorption of phosphate in anoxic marine sediments 1. *Limnology and oceanography* **25**, 797–806.

Krom M. D. and Berner R. A. (1981) The diagenesis of phosphorus in a nearshore marine sediment. *Geochimica et Cosmochimica Acta* **45**, 207–216.

Krom M., Kress N., Brenner S. and Gordon L. (1991) Phosphorus limitation of primary productivity in the eastern Mediterranean Sea. *Limnology and Oceanography* **36**, 424–432.

Kubeneck L. J., Lenstra W. K., Malkin S. Y., Conley D. J. and Slomp C. P. (2021) Phosphorus burial in vivianite-type minerals in methane-rich coastal sediments. *Marine Chemistry* **231**, 103948.

Kump L. R. (2008) The rise of atmospheric oxygen. *Nature* **451**, 277.

Laakso T. A. and Schrag D. P. (2014) Regulation of atmospheric oxygen during the Proterozoic. *Earth and Planetary Science Letters* **388**, 81–91.

Laakso T. A., Sperling E. A., Johnston D. T. and Knoll A. H. (2020) Ediacaran reorganization of the marine phosphorus cycle. *Proceedings of the National Academy of Sciences* **117**, 11961–11967.

Lenton T. M., Boyle R. A., Poulton S. W., Shields-Zhou G. A. and Butterfield N. J. (2014) Co-evolution of eukaryotes and ocean oxygenation in the Neoproterozoic era. *Nature Geosci* **7**, 257–265.

Lenton T. M. and Daines S. J. (2017) Biogeochemical transformations in the history of the ocean. *Annual review of marine science* **9**, 31–58.

Lenton T. M. and Watson A. J. (2000) Redfield revisited: 1. Regulation of nitrate, phosphate, and oxygen in the ocean. *Global biogeochemical cycles* **14**, 225–248.

Li Y.-L., Konhauser K. O. and Zhai M. (2017) The formation of magnetite in the early Archean oceans. *Earth and Planetary Science Letters* **466**, 103–114.

Liu A. G., Mcllroy D. and Brasier M. D. (2010) First evidence for locomotion in the Ediacara biota from the 565 Ma Mistaken Point Formation, Newfoundland. *Geology* **38**, 123–126.

Liu J., Izon G., Wang J., Antler G., Wang Z., Zhao J. and Egger M. (2018) Vivianite formation in methane-rich deep-sea sediments from the South China Sea. *Biogeosciences* **15**, 6329–6348.

Lomas M. W., Burke A. L., Lomas D. A., Bell D. W., Shen C., Dyhrman S. T. and Ammerman J. W. (2010) Sargasso Sea phosphorus biogeochemistry: an important role for dissolved organic phosphorus (DOP). *Biogeosciences* **7**, 695–710.

Lyons T. W., Reinhard C. T. and Planavsky N. J. (2014) The rise of oxygen in Earth/'s early ocean and atmosphere. *Nature* **506**, 307–315.

Maliva R. G., Knoll A. H. and Simonson B. M. (2005) Secular change in the Precambrian silica cycle: insights from chert petrology. *Geological Society of America Bulletin* **117**, 835–845.

Martin W., Rotte C., Hoffmeister M., Theissen U., Gelius-Dietrich G., Ahr S. and Henze K. (2003) Early cell evolution, eukaryotes, anoxia, sulfide, oxygen, fungi first (?), and a tree of genomes revisited. *IUBMB life* **55**, 193–204.

März C., Riedinger N., Sena C. and Kasten S. (2018) Phosphorus dynamics around the sulphate-methane transition in continental margin sediments: Authigenic apatite and Fe (II) phosphates. *Marine Geology* **404**, 84–96.

Mort H. P., Slomp C. P., Gustafsson B. G. and Andersen T. J. (2010) Phosphorus recycling and burial in Baltic Sea sediments with contrasting redox conditions. *Geochimica et Cosmochimica Acta* **74**, 1350–1362.

Muhling J. R. and Rasmussen B. (2020) Widespread deposition of greenalite to form banded iron formations before the Great Oxidation Event. *Precambrian Research* **339**, 105619.

Murray J. W., Jannasch H. W., Honjo S., Anderson R. F., Reeburgh W. S., Top Z., Friederich G. E., Codispoti L. A. and Izdar E. (1989) Unexpected changes in the oxic/anoxic interface in the Black Sea. *Nature* **338**, 411–413.

Och L. M. and Shields-Zhou G. A. (2012) The Neoproterozoic oxygenation event: environmental perturbations and biogeochemical cycling. *Earth-Science Reviews* **110**, 26–57.

O'Connell D. W., Mark Jensen M., Jakobsen R., Thamdrup B., Joest Andersen T., Kovacs A. and Bruun Hansen H. C. (2015) Vivianite formation and its role in phosphorus retention in Lake Ørn, Denmark. *Chemical Geology* **409**, 42–53.

Olson S. L., Kump L. R. and Kasting J. F. (2013) Quantifying the areal extent and dissolved oxygen concentrations of Archean oxygen oases. *Chemical Geology* **362**, 35–43.

Papineau D. (2010) Global Biogeochemical Changes at Both Ends of the Proterozoic: Insights from Phosphorites. *Astrobiology* **10**, 165–181.

Peiffer S., Dos Santos Afonso M., Wehrli B. and Gaechter R. (1992) Kinetics and mechanism of the reaction of hydrogen sulfide with lepidocrocite. *Environmental science & technology* **26**, 2408–2413.

Planavsky N. J. (2014) The elements of marine life. *Nature Geoscience* **7**, 855–856.

Planavsky N. J., Asael D., Rooney A. D., Robbins L. J., Gill B. C., Dehler C. M., Cole D. B., Porter S. M., Love G. D. and Konhauser K. O. (2023) A sedimentary record of the evolution of the global marine phosphorus cycle. *Geobiology* **21**, 168–174.

Planavsky N. J., McGoldrick P., Scott C. T., Li C., Reinhard C. T., Kelly A. E., Chu X., Bekker A., Love G. D. and Lyons T. W. (2011) Widespread iron-rich conditions in the mid-Proterozoic ocean. *Nature* **477**, 448–451.

Planavsky N. J., Reinhard C. T., Wang X., Thomson D., McGoldrick P., Rainbird R. H., Johnson T., Fischer W. W. and Lyons T. W. (2014) Low Mid-Proterozoic atmospheric oxygen levels and the delayed rise of animals. *science* **346**, 635–638.

Planavsky N. J., Rouxel O. J., Bekker A., Lalonde S. V., Konhauser K. O., Reinhard C. T. and Lyons T. W. (2010) The evolution of the marine phosphate reservoir. *Nature* **467**, 1088–1090.

Poulton S. W. (2017) Biogeochemistry: Early phosphorus redigested. *Nature Geoscience* **10**, 75.

Poulton S. W. (2003) Sulfide oxidation and iron dissolution kinetics during the reaction of dissolved sulfide with ferrihydrite. *Chemical Geology* **202**, 79–94.

Poulton S. W., Bekker A., Cumming V. M., Zerkle A. L., Canfield D. E. and Johnston D. T. (2021) A 200-million-year delay in permanent atmospheric oxygenation. *Nature* **592**, 232–236.

Poulton S. W. and Canfield D. E. (2005) Development of a sequential extraction procedure for iron: implications for iron partitioning in continentally derived particulates. *Chemical Geology* **214**, 209–221.

Poulton S. W. and Canfield D. E. (2011) Ferruginous Conditions: A Dominant Feature of the Ocean through Earth's History. *Elements* **7**, 107–112.

Poulton S. W., Fralick P. W. and Canfield D. E. (2010) Spatial variability in oceanic redox structure 1.8 billion years ago. *Nature Geosci* **3**, 486–490.

Poulton S. W., Fralick P. W. and Canfield D. E. (2004a) The transition to a sulphidic ocean 1.84 billion years ago. *Nature* **431**, 173–177.

Poulton S. W., Krom M. D. and Raiswell R. (2004b) A revised scheme for the reactivity of iron (oxyhydr) oxide minerals towards dissolved sulfide. *Geochimica et Cosmochimica Acta* **68**, 3703–3715.

Pyzik A. J. and Sommer S. E. (1981) Sedimentary iron monosulfides: kinetics and mechanisms of formation. *Geochim. Cosmochim. Acta* **45**.

Rasmussen B, Muhling J. and Krapež B. (2021) Greenalite and its role in the genesis of early Precambrian iron formations–A review. *Earth-Science Reviews* **217**, 103613.

Rasmussen Birger, Muhling J. R., Suvorova A. and Fischer W. W. (2021) Apatite nanoparticles in 3.46–2.46 Ga iron formations: Evidence for phosphorus-rich hydrothermal plumes on early Earth. *Geology* **49**, 647–651.

Rasmussen B., Muhling J. R., Tosca N. J. and Fischer W. W. (2023) Did nutrient-rich oceans fuel Earth's oxygenation? *Geology* **51**, 444–448.

Rasmussen B., Muhling J. R., Tosca N. J. and Tsikos H. (2019) Evidence for anoxic shallow oceans at 2.45 Ga: Implications for the rise of oxygenic photosynthesis. *Geology* **47**, 622–626.

Redfield A. C. (1958) The biological control of chemical factors in the environment. *American scientist*, 230A–221.

Rego E. S., Busigny V., Lalonde S. V., Rossignol C., Babinski M. and Philippot P. (2023) Low-phosphorus concentrations and important ferric hydroxide scavenging in Archean seawater. *PNAS Nexus* **2**, pgad025.

Reinhard C. T., Planavsky N. J., Gill B. C., Ozaki K., Robbins L. J., Lyons T. W., Fischer W. W., Wang C., Cole D. B. and Konhauser K. O. (2017) Evolution of the global phosphorus cycle. *Nature* **541**, 386.

Rivas-Lamelo S., Benzerara K., Lefèvre C., Monteil C., Jézéquel D., Menguy N., Viollier E., Guyot F., Férard C. and Poinsot M. (2017) Magnetotactic bacteria as a new model for P sequestration in the ferruginous Lake Pavin.

Rosing M. T., Rose N. M., Bridgwater D. and Thomsen H. S. (1996) Earliest part of Earth's stratigraphic record: A reappraisal of the >3.7 Ga Isua (Greenland) supracrustal sequence. *Geology* **24**, 43–46.

Rotaru A.-E., Posth N. R., Löscher C. R., Miracle M. R., Vicente E., Cox R. P., Thompson J., Poulton S. W. and Thamdrup B. (2019) Interspecies interactions mediated by conductive minerals in the sediments of the iron rich meromictic Lake La Cruz, Spain. *Limnetica* **38**, 21–40.

Rudnick R. and Gao S. (2003) Composition of the continental crust. *Treatise on geochemistry* **3**, 1–64.

Ruttenberg K. (2003) The global phosphorus cycle. *Treatise on geochemistry* **8**, 682.

Ruttenberg K. C. (1992) Development of a sequential extraction method for different forms of phosphorus in marine sediments. *Limnology and Oceanography* **37**, 1460–1482.

Ruttenberg K. C. and Berner R. A. (1993) Authigenic apatite formation and burial in sediments from non-upwelling, continental margin environments. *Geochimica et cosmochimica acta* **57**, 991–1007.

Ruttenberg K. and Canfield D. (1994) Chemical distribution of phosphorus in suspended particulate matter from twelve North American rivers: evidence for bioavailability of particulate-P. *EOS* **75**, 110.

Ruttenberg K. and Goni M. (1997) Phosphorus distribution, C: N: P ratios, and δ13Coc in arctic, temperate, and tropical coastal sediments: tools for characterizing bulk sedimentary organic matter. *Marine Geology* **139**, 123–145.

Schad M., Halama M., Jakus N., Robbins L. J., Warchola T. J., Tejada J., Kirchhof R., Lalonde S. V., Swanner E. D. and Planavsky N. J. (2021) Phosphate remobilization from banded iron formations during metamorphic mineral transformations. *Chemical Geology* **584**, 120489.

Schopf J. W. (1993) Microfossils of the Early Archean Apex chert: New evidence of the antiquity of life. *Science* **260**, 640–646.

Scott C., Lyons T. W., Bekker A., Shen Y., Poulton S. W., Chu X. and Anbar A. D. (2008) Tracing the stepwise oxygenation of the Proterozoic ocean. *Nature* **452**, 456–459.

Slomp C. P., Epping E., Helder W. and Raaphorst W. (1996a) A key role for iron-bound phosphorus in authigenic apatite formation in North Atlantic continental platform sediments. *Journal of marine Research* **54**, 1179–1205.

Slomp C. P., Mort H. P., Jilbert T., Reed D. C., Gustafsson B. G. and Wolthers M. (2013) Coupled dynamics of iron and phosphorus in sediments of an oligotrophic coastal basin and the impact of anaerobic oxidation of methane. *PloS one* **8**, e62386.

Slomp C. P., Thomson J. and de Lange G. J. (2004) Controls on phosphorus regeneration and burial during formation of eastern Mediterranean sapropels. *Marine Geology* **203**, 141–159.

Slomp C. P., Van der Gaast S. and Van Raaphorst W. (1996b) Phosphorus binding by poorly crystalline iron oxides in North Sea sediments. *Marine Chemistry* **52**, 55–73.

Slomp C. and Van Cappellen P. (2007) The global marine phosphorus cycle: sensitivity to oceanic circulation. *Biogeosciences* **4**, 155–171.

Sperling E. A. and Stockey R. G. (2018) The Temporal and Environmental Context of Early Animal Evolution: Considering All the Ingredients of an "Explosion." *Integrative and Comparative Biology* **58**, 605–622.

Sperling E. A., Wolock C. J., Morgan A. S., Gill B. C., Kunzmann M., Halverson G. P., Macdonald F. A., Knoll A. H. and Johnston D. T. (2015) Statistical analysis of iron geochemical data suggests limited late Proterozoic oxygenation. *Nature* **523**, 451–454.

Teng Y.-C., Primeau F. W., Moore J. K., Lomas M. W. and Martiny A. C. (2014) Global-scale variations of the ratios of carbon to phosphorus in exported marine organic matter. *Nature Geoscience* **7**, 895.

Thompson J. (2018) Iron and phosphorus cycling under ferruginous conditions. Ph.D Thesis, University of Leeds, UK.

Thompson J., Poulton S. W., Guilbaud R., Doyle K. A., Reid S. and Krom M. D. (2019) Development of a modified SEDEX phosphorus speciation method for ancient rocks and modern iron-rich sediments. *Chemical Geology* **524**, 383–393.

Thomson D., Rainbird R. H., Planavsky N., Lyons T. W. and Bekker A. (2015) Chemostratigraphy of the Shaler Supergroup, Victoria Island, NW Canada: A record of ocean composition prior to the Cryogenian glaciations. *Precambrian Research* **263**, 232–245.

Tosca N. J., Guggenheim S. and Pufahl P. K. (2016) An authigenic origin for Precambrian greenalite: Implications for iron formation and the chemistry of ancient seawater. *Bulletin* **128**, 511–530.

Tostevin R., Clarkson M. O., Gangl S., Shields G. A., Wood R. A., Bowyer F., Penny A. M. and Stirling C. H. (2019) Uranium isotope evidence for an expansion of anoxia in terminal Ediacaran oceans. *Earth and Planetary Science Letters* **506**, 104–112.

Tostevin R., Wood R. A., Shields G. A., Poulton S. W., Guilbaud R., Bowyer F., Penny A. M., He T., Curtis A., Hoffmann K. H. and Clarkson M. O. (2016) Low-oxygen waters limited habitable space for early animals. *Nature Communications* **7**, 12818.

Treguer P., Nelson D. M., Van Bennekom A. J., DeMaster D. J., Leynaert A. and Quéguiner B. (1995) The silica balance in the world ocean: a reestimate. *Science* **268**, 375–379.

Turekian K. K. and Wedepohl K. H. (1961) Distribution of the Elements in Some Major Units of the Earth's Crust. *Geological Society of America Bulletin* **72**, 175–192.

Tyrrell T. (1999) The relative influences of nitrogen and phosphorus on oceanic primary production. *Nature* **400**, 525.

Van Cappellen P. and Ingall E. D. (1994) Benthic phosphorus regeneration, net primary production, and ocean anoxia: A model of the coupled marine biogeochemical cycles of carbon and phosphorus. *Paleoceanography* **9**, 677–692.

Vuillemin A., Ariztegui D., De Coninck A., Lücke A., Mayr C., Schubert C. J., and PASADO Scientific Team (2013) Origin and significance of diagenetic concretions in sediments of Laguna Potrok Aike, southern Argentina. *Journal of paleolimnology* **50**, 275–291.

Vuillemin A., Friese A., Wirth R., Schuessler J. A., Schleicher A. M., Kemnitz H., Lücke A., Bauer K. W., Nomosatryo S. and Von Blanckenburg F. (2020) Vivianite formation in ferruginous sediments from Lake Towuti, Indonesia. *Biogeosciences* **17**, 1955–1973.

Vuillemin A., Friese A., Wirth R., Schuessler J., Schleicher A., Kemnitz H., Lücke A., Bauer K., Nomosatryo S. and Blanckenburg F. (2019) Vivianite formation in ferruginous sediments from Lake Towuti. *Indonesia. Biogeosciences Discuss.* **2019**, 1–26.

Wacey D., Battison L., Garwood R. J., Hickman-Lewis K. and Brasier M. D. (2017) Advanced analytical techniques for studying the morphology and chemistry of Proterozoic microfossils. *Geological Society, London, Special Publications* **448**, 81–104.

Wheat C. G., Feely R. A. and Mottl M. J. (1996) Phosphate removal by oceanic hydrothermal processes: An update of the phosphorus budget in the oceans. *Geochimica et Cosmochimica Acta* **60**, 3593–3608.

Wood R., Poulton S., Prave A., Hoffmann K.-H., Clarkson M., Guilbaud R., Lyne J., Tostevin R., Bowyer F. and Penny A. (2015) Dynamic redox conditions control late Ediacaran metazoan ecosystems in the Nama Group, Namibia. *Precambrian Research* **261**, 252–271.

Xiong Y., Guilbaud R., Peacock C. L., Cox R. P., Canfield D. E., Krom M. D. and Poulton S. W. (2019) Phosphorus cycling in Lake Cadagno, Switzerland: A low sulfate euxinic ocean analogue. *Geochimica et Cosmochimica Acta* **251**, 116–135.

Xiong Y., Guilbaud R., Peacock C. L., Krom M. D. and Poulton S. W. (2023) Phosphorus controls on the formation of vivianite versus green rust under anoxic conditions. *Geochimica et Cosmochimica Acta* **351**, 139–151.

Zegeye A., Bonneville S., Benning L. G., Sturm A., Fowle D. A., Jones C., Canfield D. E., Ruby C., MacLean L. C., Nomosatryo S., Crowe S. A. and Poulton S. W. (2012) Green rust formation controls nutrient availability in a ferruginous water column. *Geology* **40**, 599–602.

Zhang F., Algeo T. J., Romaniello S. J., Cui Y., Zhao L., Chen Z.-Q. and Anbar A. D. (2018) Congruent Permian-Triassic δ238U records at Panthalassic and Tethyan sites: Confirmation of global-oceanic anoxia and validation of the U-isotope paleoredox proxy. *Geology* **46**, 327–330.

Zhang S., Wang X., Wang H., Bjerrum C. J., Hammarlund E. U., Costa M. M., Connelly J. N., Zhang B., Su J. and Canfield D. E. (2016) Sufficient oxygen for animal respiration 1,400 million years ago. *Proceedings of the National Academy of Sciences* **113**, 1731–1736.

Zhu S., Zhu M., Knoll A. H., Yin Z., Zhao F., Sun S., Qu Y., Shi M. and Liu H. (2016) Decimetre-scale multicellular eukaryotes from the 1.56-billion-year-old Gaoyuzhuang Formation in North China. *Nature communications* **7**, 11500.

Figures

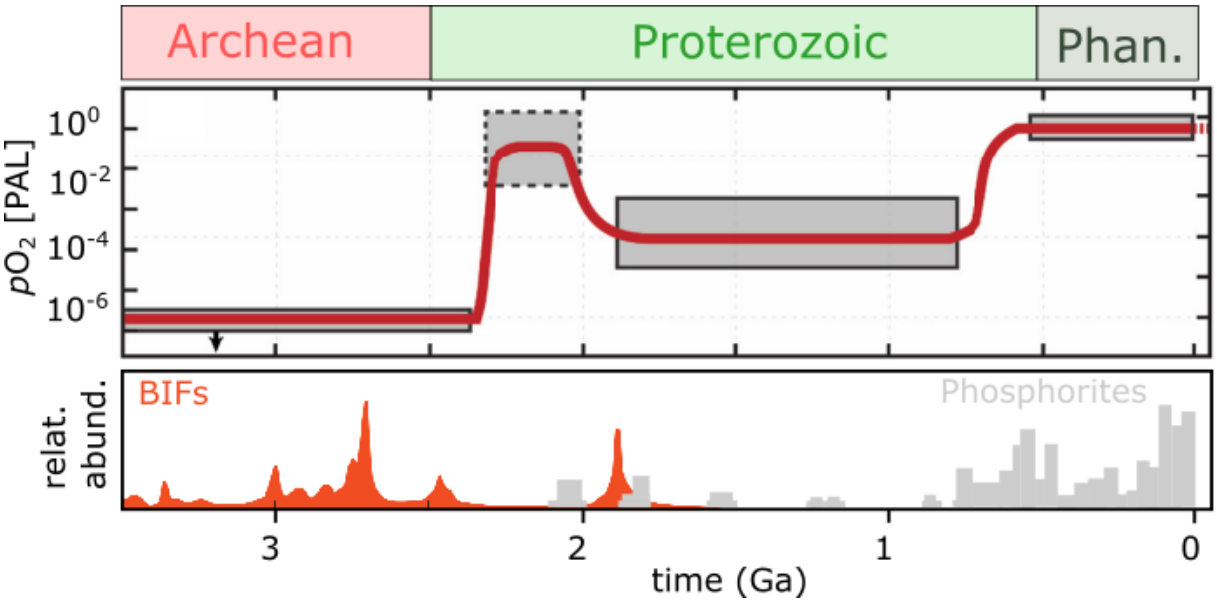

Figure 1. Reconstruction of atmospheric O_2 evolution (upper panel) and the deposition of banded iron formations (BIFs, red) and phosphorites (grey) through geologic times (down), modified after Planavsky (2014) and Planavsky et al. (2023). Note that pO_2 is expressed as a function of present atmospheric levels [PAL]. Grey squares represent model uncertainties on atmospheric O_2 levels. Phosphorite data (Holland, 2005) and BIFs data (Isley and Abbott, 1999) are expressed in relative abundances but with different scales (i.e., heights in BIFs abundances do not compare with heights in phosphorite abundances).

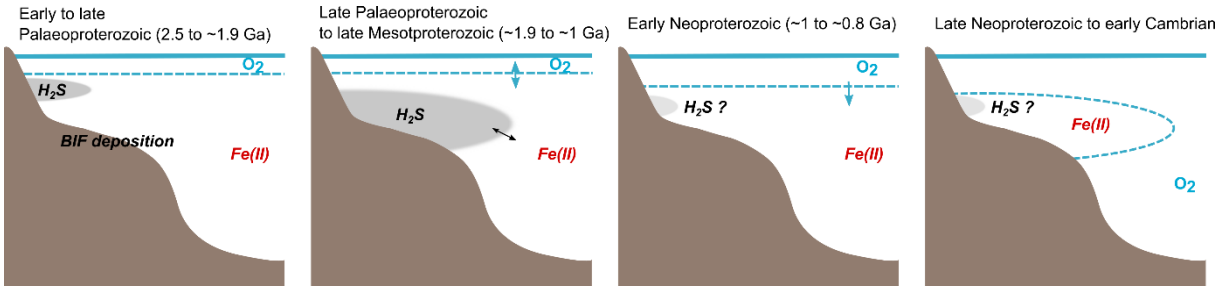

Figure 2. Schematic of the redox evolution of the Precambrian oceans depicting the development of euxinic continental margins, and the progressive retraction of anoxia until the ventilation of the deep ocean at the end of the Proterozoic, modified after Poulton and Canfield (2011), and Guilbaud et al. (2015, 2018).

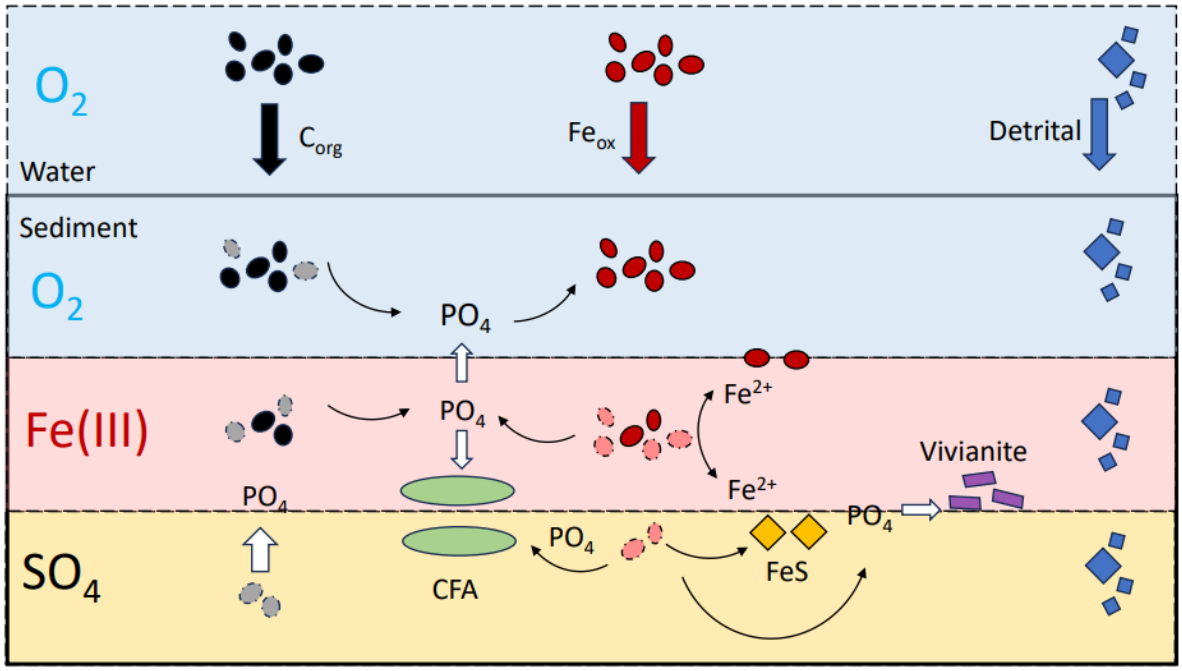

Figure 3. Simplified, schematic cartoon of the coupled iron-phosphorous cycle in sediments that undergo a range of redox conditions, from oxic environments at the sediment-water interface, ferruginous environments where Fe(III) (oxyhydr)oxides become the major electron acceptor, and down to sulphidic environments where sulphate reduction occurs, producing sulphide. In the water column, the main P carriers to the sediment include organic matter (C_{org}), Fe (oxyhydr)oxides (Fe_{ox}) and detrital apatite (note that authigenic water column particles and dust are not represented). Well-crystalline, detrital apatite remains unreactive throughout deposition and burial. Within oxic sediments, organic matter gets partially remineralised, liberating P that may re-adsorb onto Fe minerals. Within ferruginous sediments, whilst C_{org} respiration continues, Fe reduction occurs producing Fe^{2+}, which may react with phosphate to form CFA or vivianite. Within sulphidic sediments, P release from C_{org} is enhanced, and Fe dissolution by sulphide also occurs, further releasing P, which may precipitate as CFA, or diffuse upwards to precipitate as vivianite or reach the water column.

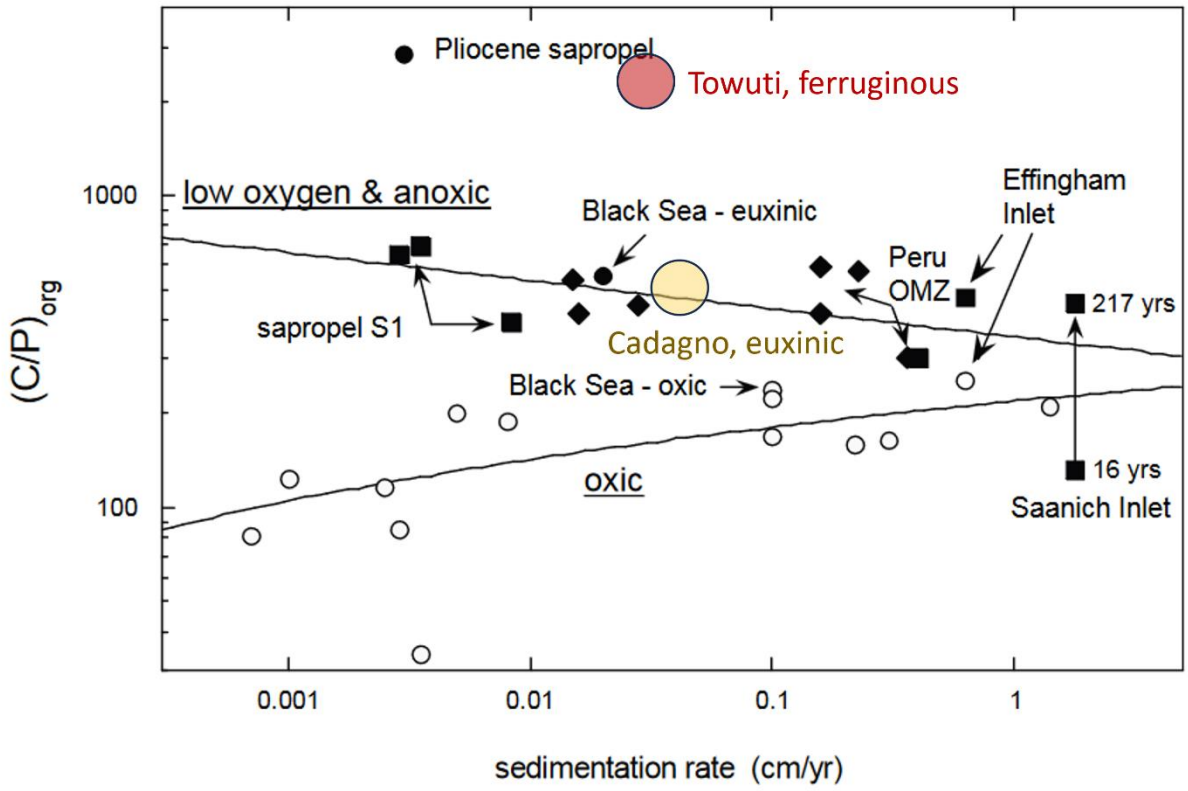

Figure 4. Compilation of C_{org}/P_{org} in a range of sediments, after Slomp and Van Cappellen (2007). Oxic sediments are illustrated by open circles, low-oxygen environments by closed diamonds, ferruginous environments by closed squares and euxinic/sulphidic sediments by closed circles. Complementary data from ferruginous Lake Towuti (Vuillemin et al., 2020) and euxinic Lake Cadagno (Xiong et al., 2019) are in red and yellow, respectively.

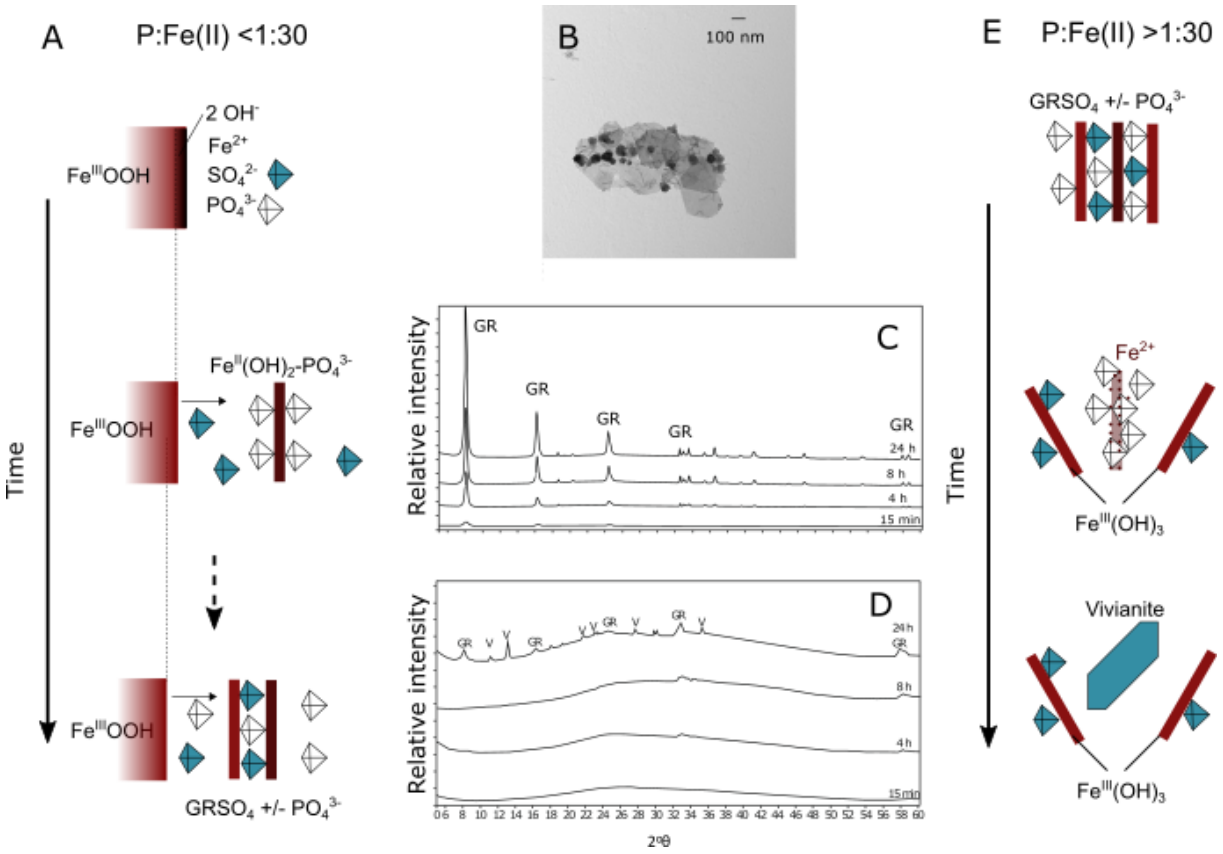

Figure 5. Mechanism of green rust (GR) versus vivianite (V) formation through time, with varying P concentrations. (A) GR rapidly crystallises (*via* an FeOOH precursor, while Fe^{2+} and sulphate, represented by the blue tetrahedra, remain in solution). Phosphate (represented by the white tetrahedra) associates with neo-formed $Fe(OH)_2$ clusters, delaying the crystallisation of GR, which eventually forms and incorporates phosphate as interlayer anions. (B) TEM image showing the formation of green rust (with their typical hexagonal shape). (C) XRD spectra of experimental mineralogical products obtained when P:Fe(II) <30, i.e. green rust only. (D) XRD spectra of experimental mineralogical products obtained when P:Fe(II) >30, i.e. a mixture of green rust and vivianite. (E) Proposed mechanism for the dissolution of PO_3-bearing green rust and the precipitation of vivianite and amorphous $Fe(OH)_3$. Modified after Xiong et al. (2023).

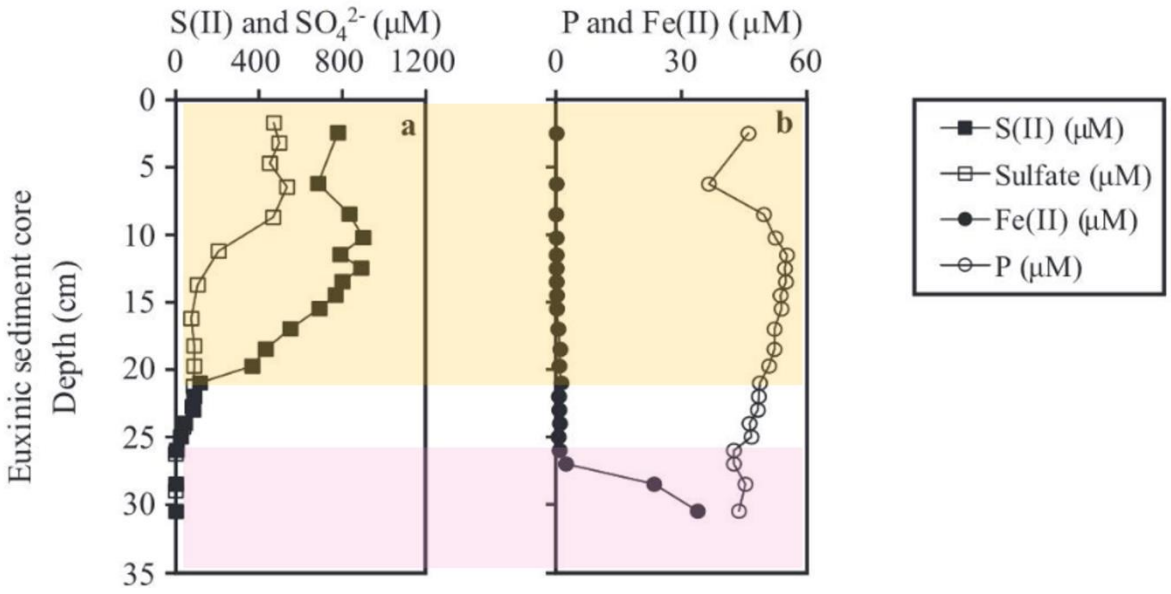

Figure 6. Porewater geochemical profiles of sediments deposited under low-sulphate, euxinic conditions, after Xiong et al. (2019). The orange shade represents the sulphidic sediment, whereas the pink shade is for the ferruginous sediment where sulphide depletion allows for Fe(II) build up. Production of dissolved P and Fe^{2+} at depth favour the supersaturation conditions for vivianite formation.

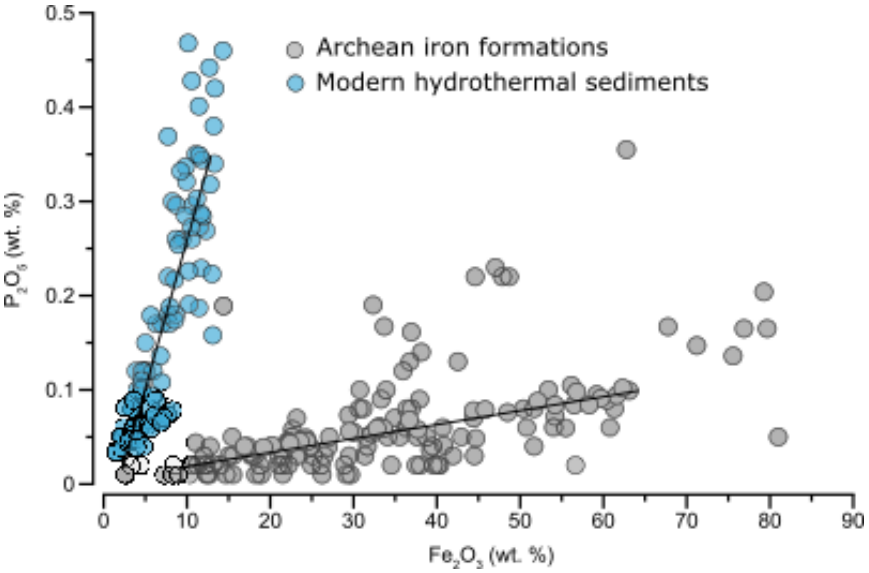

Figure 7. Linear relationship between P_2O_5 and Fe_2O_3 in modern hydrothermal vents (in blue) and Archean iron formations (in grey), modified after (Rego et al., 2023).

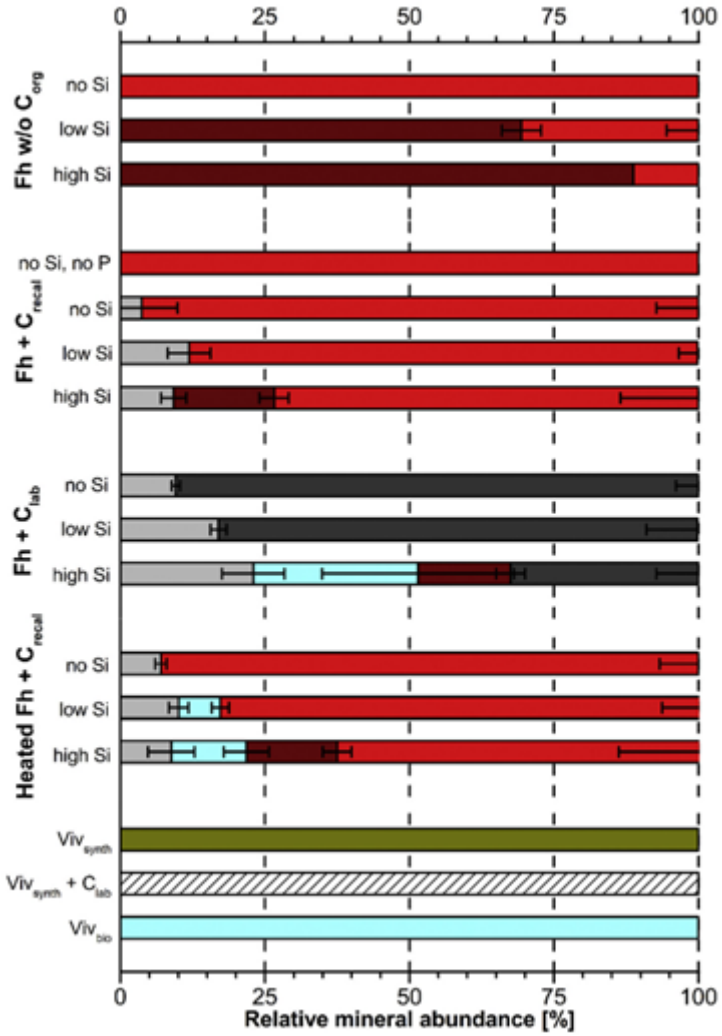

Figure 8. Mineralogical products of BIF-genesis simulating experiments, with or without silica, modified after (Schad et al., 2021). 'Fh' stands for ferrihydrite, 'Viv' for vivianite; 'C_{lab}' for labile organic matter and C_{recal}' for recalcitrant organic matter in the starting conditions. Relative abundances of final products are depicted by coloured bars, with dark red for ferrihydrite, bright red for hematite, light grey for siderite, dark grey for magnetite, blue for vivianite and green for phosphoferrite, a dehydrated Fe phosphate.

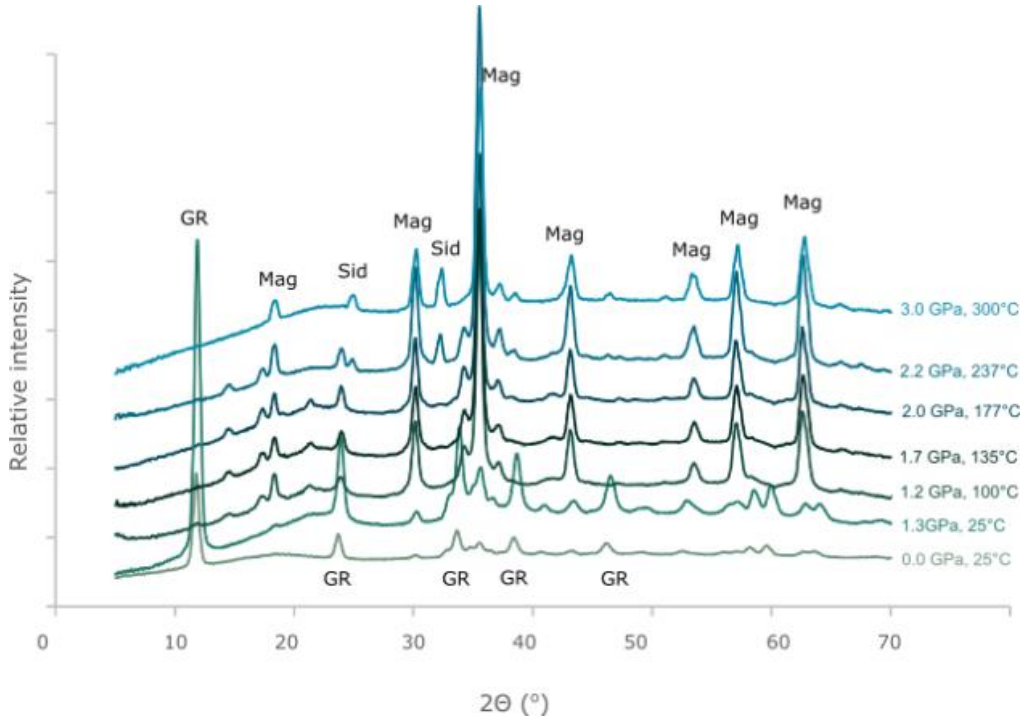

Figure 9. XRD spectra of *in-situ* analysis of P-T experiments (0-3 GPa and 0-300°C) simulating the diagenesis and metamorphism of carbonated green rust (GR = green rust). Mineralogical transformations involve the formation of magnetite (Mag) and siderite (Sid).

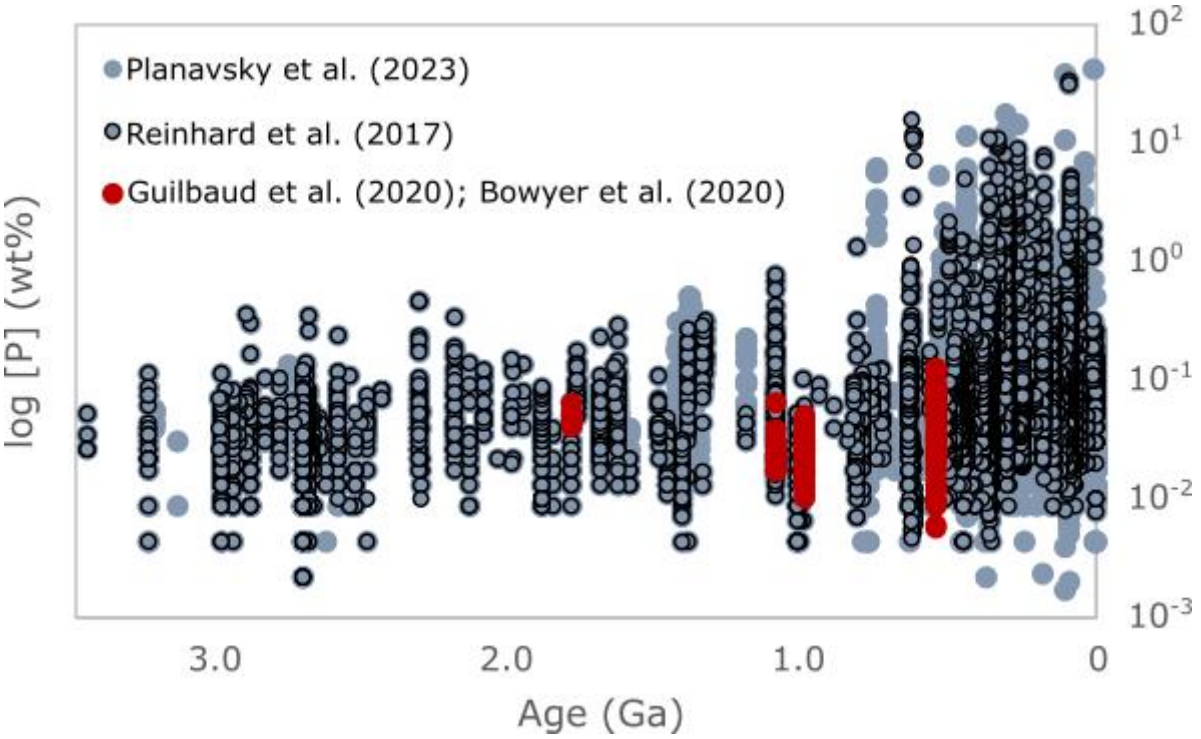

Figure 10. Compilation of P contents in shales through time, after Reinhard et al. (2017) and Planavsky et al. (2023) and augmented by Guilbaud et al. (2020) and Bowyer et al. (2020). Note that sedimentary P contents are expressed on a log scale.

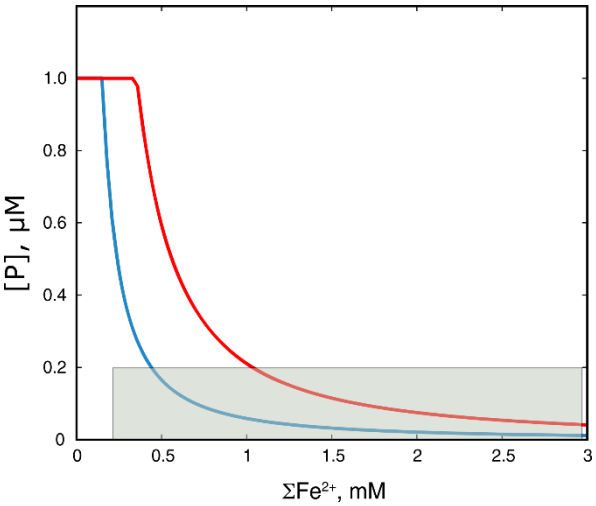

Figure 11. Total dissolved P as a function of total dissolved Fe^{2+} in equilibrium with vivianite at pH 8 (blue) and pH 7.5 (red). The shaded area represents presumed Proterozoic conditions, with [P] <0.2 µM, assuming that P removal *via* vivianite dominates. Modified after Derry (2015).

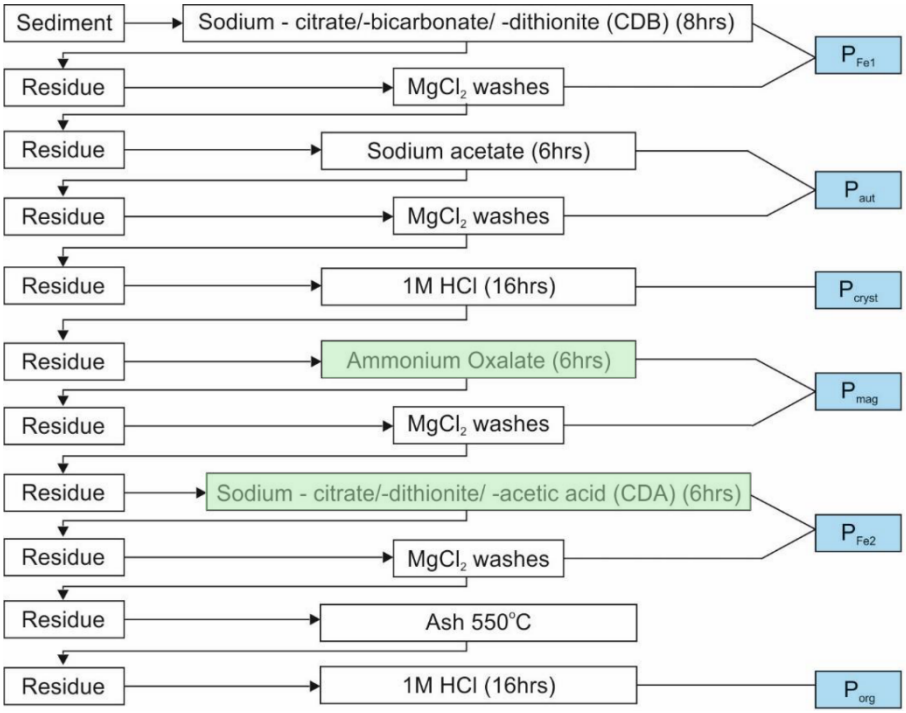

Figure 12. Revised extraction scheme addressing the speciation of P in ancient sedimentary rocks (Thompson et al., 2019). Highlighted in green are the specific steps targeting P_{mag} and P_{Fe2}, from the Fe speciation method (Poulton and Canfield, 2005).

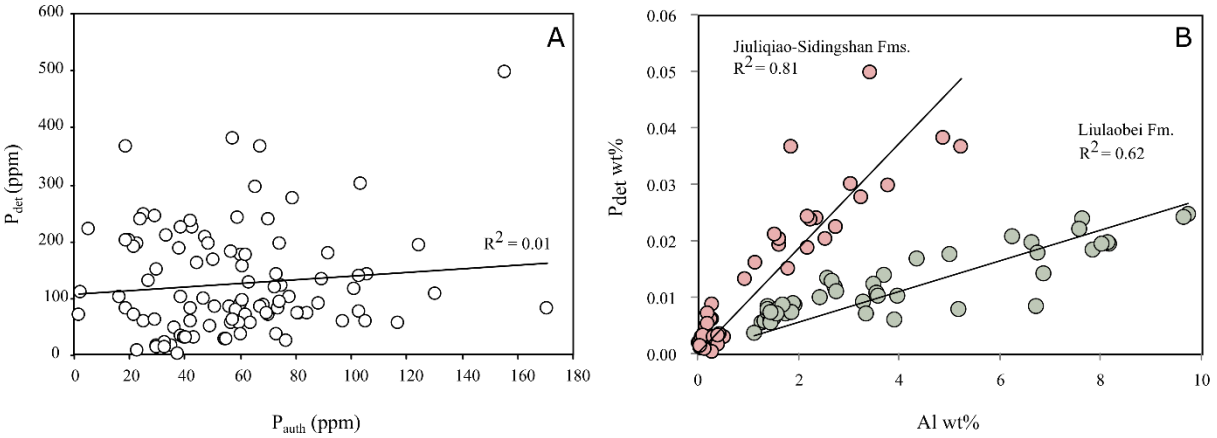

Figure 13. Data quality checks performed on the ~1 Ga Jiuliqiao-Sidingshan succession and the Liulaobei Formation, Huainan Basin, North China craton, modified after Guilbaud et al. (2020). The clear correlations between P_{det} and Al (B) testify that P_{det} indeed represents detrital apatite.

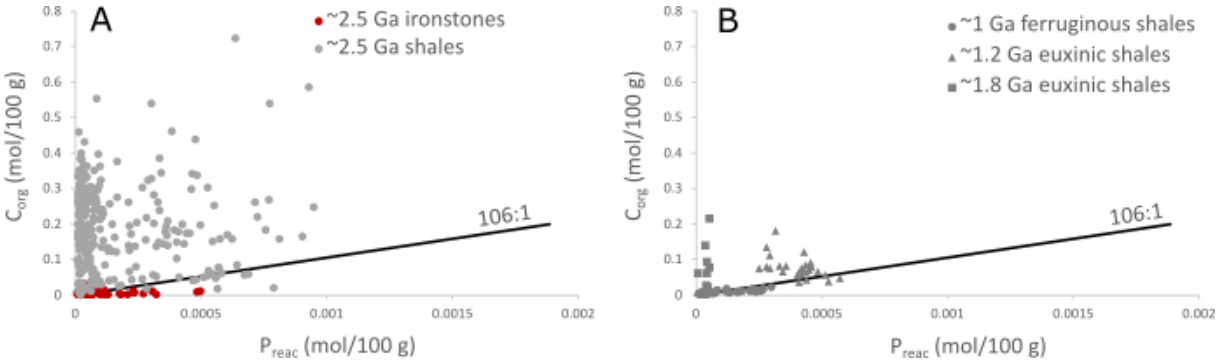

Figure 14. C_{org} versus P_{reac} for ~2.5 Ga shales and ironstones from the Campbellrand and Koegas Subgroups, South Africa (A), and for ~1 Ga shales from the Huainan Basin, North China (B). The black line represents the Redfield ratio of 106:1. Shale data from the ~2.5 Ga successions suggest strong sulphide-induced P recycling, whilst data from later Proterozoic euxinic shales seem to suggest less intense recycling. By contrast, ironstones and ~1 Ga ferruginous shales data are close or below the Redfiled ration, suggesting efficient P fixation in the sediment. Data are from Alcott et al. (2022) and Guilbaud et al. (2020).

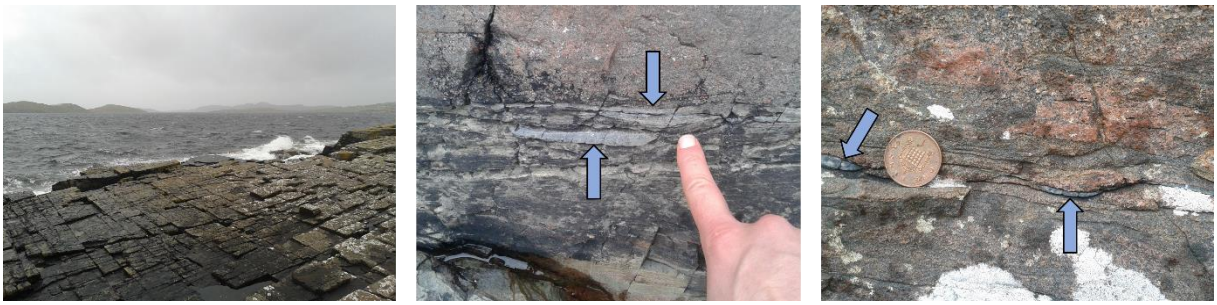

Figure 15. Outcrops photographs of the ~1 Ga uppermost Diabaig Formation, Torridon Group, Scotland. The blue arrows point towards phosphatic lenses within lacustrine sands and Fe-rich siltstones.

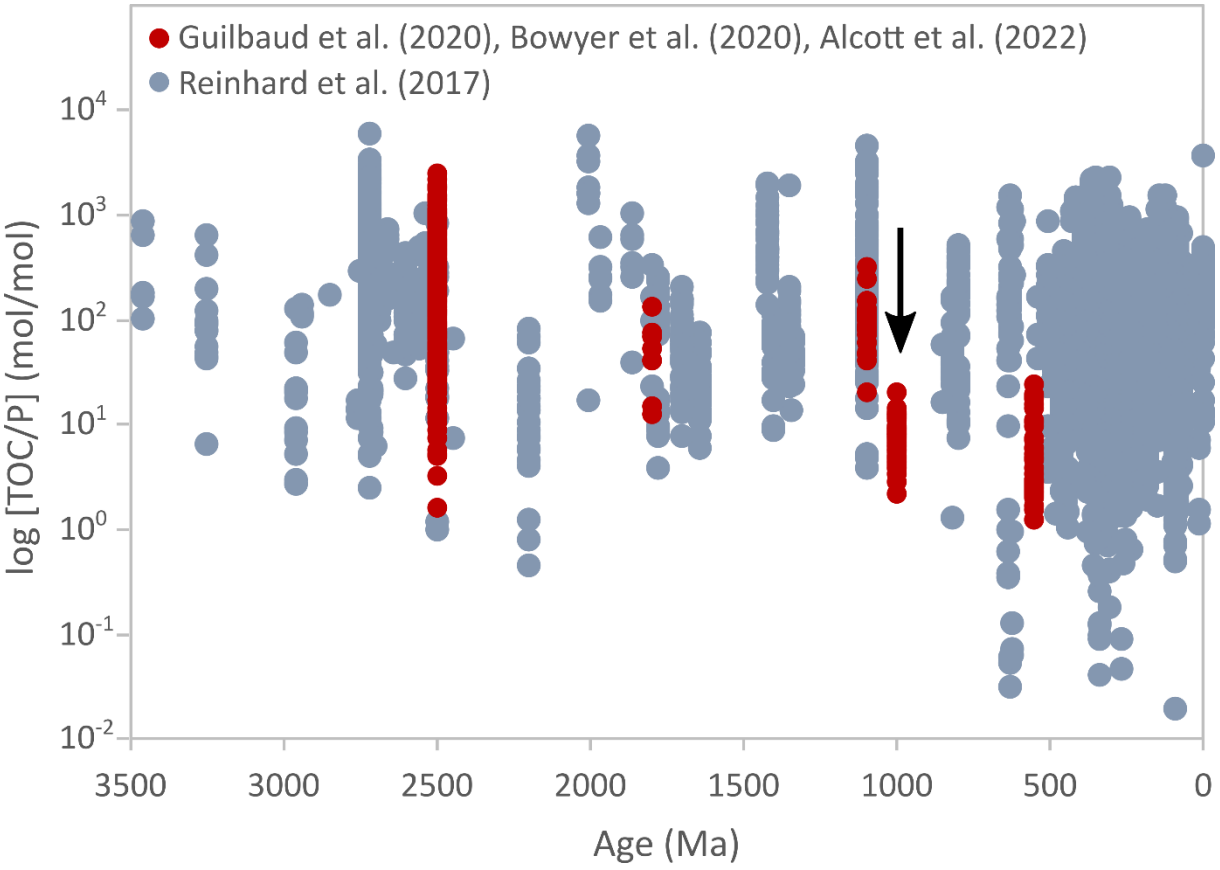

Figure 16. Compilation of TOC/P ratios in shales through time (note the log scale). The black arrows represent sharp decreases in TOC/P in ferruginous shales at ~1 Ga (Guilbaud et al., 2020; Alcott et al., 2022). Note that ironstone data from Alcott et al. (2022) were omitted for lithological consistency.

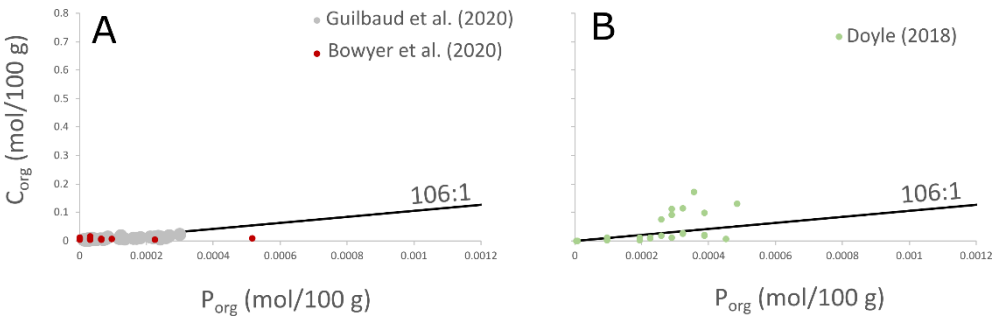

Figure 17. (A) C_{org} versus P_{org} in ferruginous and oxic Neoproterozoic sediments with vanishingly low sulphide (Guilbaud et al., 2020; Bowyer et al., 2020), and (B) for ~1.6 Ga ferruginous shales filtered for sulphide contents <0.05 wt% (Doyle, 2018).

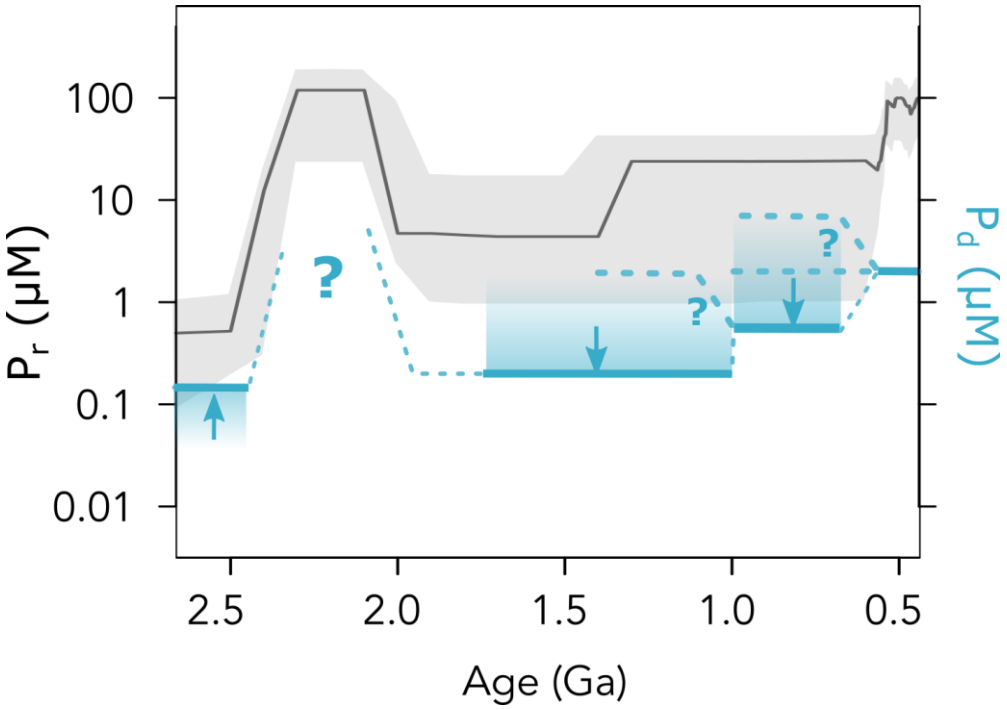

Figure 18. Reconstruction of modelled recycled P (P_r) flux to the deep ocean in black and its uncertainty (Kipp and Stüeken, 2017), and putative deep ocean P concentrations in blue. The difference between both rises from the fact that most parts of recycled P due to sulphide production may be trapped back under ferruginous water columns, contrasting with oxygenated oceans. Solid blue lines represent experimental or model constraints (Derry, 2015; Jones et al., 2015; Guilbaud et al., 2020) and arrows indicate whether these constraints are maximum or minimum estimates.

Tables

Location (reference)	**Redox condition of sampling**	**P:Fe(II) ratio in porewaters**	**Authigenic Fe(II)-bearing non-sulfidic minerals**
Lake Matano (Crowe 2008; Zegeye et al., 2012)	Ferruginous water column, at 118m depth	< 1:30	Green rust
Lake Matano (Crowe 2008; Bauer et al., 2020)	Anoxic sediments under ferruginous waters	Unknown	Magnetite
Lake Towuti (Bauer et al., 2020; Vuillemin et al., 2020)	Ferruginous water column directly above the sediment	< 1:500	Green rust

Lake Towuti (Vuillemin et al., 2019)	Anoxic sediments under ferruginous waters	Between 1:150 and 1:2700	Siderite, vivianite
Lake Pavin (Busigny et al., 2014; Cosmidis et al., 2014)	Ferruginous water column, at 67m depth	1:6	Vivianite
Lake Pavin (Busigny et al., 2014; Cosmidis et al., 2014)	Ferruginous water column, at 86m depth	1:3	Vivianite
Lake Cadagno (Xiong et al., 2019)	Sulfide-depleted anoxic sediments under euxinic water column	1:1.3 to 1:2	Vivianite
Black Sea (Kraal et al., 2017) (Dijkstra et al., 2014)	Sulphidic sediment under euxinic water column	Presumably < 40:1 (low Fe)	CFA, $CaCO_3$ (adsorption)
Lake Cadagno (Xiong et al., 2019)	Sulphidic sediment under euxinic water column	Presumably < 60:1 (low Fe)	CFA

Table 1. Authigenic mineralogy and P:Fe(II) ratios from a range of modern ferruginous and euxinic settings, modified after Xiong et al. (2023).

Time period	Mean C/P	Median C/P
Phanerozoic	192:1	105:1
Ediacaran	314:1	164:1
1.0-0.8 Ga	142:1	62:1
1.8-1.0 Ga	265:1	89:1
2.5-1.8 Ga	415:1	38:1

Table 2. Bulk shale C/P ratios binned as a function of time periods. Data are from Reinhard et al., (2017). Note that the median C/P ratio of compiled Phanerozoic shales corresponds to the Redfield ratio found in fresh marine organic matter.